UC Irvine
UC Irvine Previously Published Works

Title

Post-transcriptional Regulation of De Novo Lipogenesis by mTORC1-S6K1-SRPK2 Signaling

Permalink

https://escholarship.org/uc/item/2bt0k3cz

Journal

Cell, 171(7)

ISSN

0092-8674

Authors

Lee, Gina
Zheng, Yuxiang
Cho, Sungyun
et al.

Publication Date

2017-12-01

DOI

10.1016/j.cell.2017.10.037

Peer reviewed

Post-transcriptional regulation of de novo lipogenesis by mTORC1-S6K1-SRPK2 signaling

Gina Lee[1,2], **Yuxiang Zheng**[1,3,#], **Sungyun Cho**[1,#], **Cholsoon Jang**[4], **Christina England**[1], **Jamie M. Dempsey**[5], **Yonghao Yu**[6], **Xiaolei Liu**[7], **Long He**[1,2], **Paola M. Cavaliere**[1], **Andre Chavez**[1], **Erik Zhang**[7], **Meltem Isik**[8], **Anthony Couvillon**[9], **Noah E. Dephoure**[1], **T. Keith Blackwell**[8], **Jane J. Yu**[7], **Joshua D. Rabinowitz**[4], **Lewis C. Cantley**[1,3], and **John Blenis**[1,2,*]

[1]Meyer Cancer Center, Weill Cornell Medicine, New York, NY 10065, USA

[2]Department of Pharmacology, Weill Cornell Medicine, New York, NY 10065, USA

[3]Department of Medicine, Weill Cornell Medicine, New York, NY 10065, USA

[4]Lewis-Sigler Institute for Integrative Genomics and Department of Chemistry, Princeton University, Princeton, NJ 08544, USA

[5]Department of Cell Biology, Harvard Medical School, Boston, MA 02115, USA

[6]Department of Biochemistry, University of Texas Southwestern Medical Center, Dallas, TX 75390, USA

[7]Department of Internal Medicine, University of Cincinnati College of Medicine, Cincinnati, OH 45267, USA

[8]Joslin Diabetes Center and Department of Genetics, Harvard Medical School, Boston, MA 02215, USA

[9]Cell Signaling Technology, Danvers, MA 01923, USA

Summary

mTORC1 is a signal integrator and master regulator of cellular anabolic processes linked to cell growth and survival. Here we demonstrate that mTORC1 promotes lipid biogenesis via SRPK2, a key regulator of RNA-binding SR proteins. mTORC1-activated S6K1 phosphorylates SRPK2 at Ser494, which primes Ser497 phosphorylation by CK1. These phosphorylation events promote SRPK2 nuclear translocation and phosphorylation of SR proteins. Genome-wide transcriptome

*Correspondence and lead contact: job2064@med.cornell.edu (J.B.).
#Equally contributed

analysis reveals that lipid biosynthetic enzymes are among the downstream targets of mTORC1-SRPK2 signaling. Mechanistically, SRPK2 promotes SR protein binding to U1-70k to induce splicing of lipogenic pre-mRNAs. Inhibition of this signaling pathway leads to intron retention of lipogenic genes which triggers nonsense-mediated mRNA decay. Genetic or pharmacological inhibition of SRPK2 blunts de novo lipid synthesis, thereby suppressing cell growth. These results thus reveal a novel role of mTORC1-SRPK2 signaling in post-transcriptional regulation of lipid metabolism and demonstrate that SRPK2 is a potential therapeutic target for mTORC1-driven metabolic disorders.

Graphical Abstract
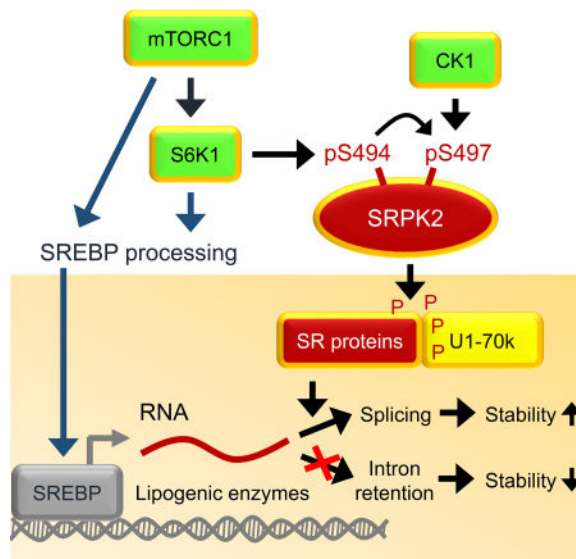
Introduction

A hallmark of living organisms is their ability to sense and couple various environmental cues to their growth. The mechanistic target of rapamycin complex 1 (mTORC1) integrates signals from growth factors, nutrients, and energy status, serving as a molecular rheostat, to regulate a wide range of anabolic and catabolic processes (Dibble and Manning, 2013; Gomes and Blenis, 2015; Saxton and Sabatini, 2017; Shimobayashi and Hall, 2014). mTORC1 is an atypical serine/threonine protein kinase that promotes cell growth through phosphorylation of multiple proteins including the ribosomal S6 kinase 1 (S6K1) and eIF4E–binding protein 1 (4E–BP1) (Ma and Blenis, 2009). Growth factors such as insulin activate PI3K–AKT signaling, thereby inhibiting the tumor suppressor tuberous sclerosis complex (TSC) 1/2, a negative regulator of mTORC1 (Manning and Toker, 2017; Shimobayashi and Hall, 2014). Loss-of-function mutations in *TSC1/2* lead to constitutive activation of mTORC1, which causes genetic tumor syndromes TSC and lymphangioleiomyomatosis (LAM) (Crino et al., 2006). Hyperactivation of mTORC1 by oncogenic PI3K-AKT and RAS-ERK pathways is also commonly observed in numerous cancers (Menon and Manning, 2008). Therefore, it is of great therapeutic importance to

better understand how mTORC1 is able to control diverse cellular processes through regulation of newly discovered downstream targets.

Cancer cells regulate synthesis of macro-molecules to support sustained proliferation (DeBerardinis and Thompson, 2012; Vander Heiden et al., 2009). De novo lipid synthesis, for instance, provides fatty acids and cholesterol for expanding cell and organelle membranes (Gonzalez Herrera et al., 2015; Menendez and Lupu, 2007). This process begins with the production of acetyl coenzyme A (acetyl-CoA) from citrate or acetate by ATP citrate lyase (ACLY) or acyl-CoA synthetase short-chain (ACSS) family members, respectively. Fatty acid synthase (FASN) then catalyzes synthesis of fatty acids using acetyl-CoA and malonyl-CoA, which is produced from acetyl-CoA by acetyl-CoA carboxylase (ACC). The resulting palmitate is then utilized to generate a number of products, such as longer fatty acids via elongation, unsaturated fatty acids via stearoyl-CoA desaturase 1 (SCD1), phospholipids, and signaling lipids. For cholesterol biosynthesis, hydroxymethylglutaryl-CoA synthase (HMGCS) catalyzes condensation of acetyl-CoA with acetoacetyl-CoA to generate HMG-CoA, which is converted to mevalonic acid by HMG-CoA reductase (HMGCR). This is then followed by multiple enzymatic reactions including those mediated by mevalonate diphosphate decarboxylase (MVD) and farnesyl diphosphate farnesyltransferase 1 (FDFT1). These key enzymes are often overexpressed in cancers (Currie et al., 2013; Menendez and Lupu, 2007). Thus, understanding the pertinent regulatory mechanisms holds promise for revealing potential therapeutic targets. One such regulator is the sterol regulatory element binding protein (SREBP) family of transcription factors, SREBP1 and 2. SREBPs are produced as inactive precursors bound to the endoplasmic reticulum membrane. Upon cellular lipid depletion, SREBPs are proteolytically processed to their active forms, translocate to the nucleus and induce transcription of target genes (Horton et al., 2002). mTORC1 increases expression of lipogenic enzymes through SREBP activation, by both inactivating its negative regulators and increasing its expression level (Duvel et al., 2010; Li et al., 2010; Owen et al., 2012; Peterson et al., 2011; Han et al., 2015). However, little is known about the post-transcriptional regulation of lipogenic enzyme expression or whether the pro-lipogenic activity of mTORC1 extends to these events.

Cells employ a wide variety of post-transcriptional mechanisms for fine-tuning mRNAs and generating proteomic diversity, such as splicing, capping, polyadenylation, methylation, nuclear export, and stability (Fabian et al., 2010; Gilbert et al., 2016; Moore and Proudfoot, 2009; Park et al., 2005). These processes are regulated in part by various RNA-binding proteins, including serine/arginine-rich (SR) proteins and heterogeneous nuclear ribonucleoproteins (hnRNPs) (Chen and Manley, 2009). SR proteins are encoded by the *serine and arginine rich splicing factor* (*SRSF*) gene family and composed of RNA recognition motifs (RRM) and arginine/serine (RS)-repeat domains. They catalyze mRNA processing by directly binding to exons in pre-mRNA and recruiting proteins such as small nuclear ribonucleoproteins (SNRNPs) (Fu and Ares, 2014; Lee and Rio, 2015). The activity of SR proteins can be regulated via phosphorylation of the RS domain by SR protein kinases (SRPKs), which alters SR protein conformation, subcellular localization and/or its interaction with other proteins (Ghosh and Adams, 2011).

Here we reveal a previously unknown layer of mTORC1-dependent regulation of lipid metabolism that utilizes a new mTORC1-regulated effector kinase, SRPK2. Mechanistically, SRPK2 controls expression of lipogenic enzymes by inducing efficient splicing of their mRNAs rather than by affecting the synthesis of transcripts. Our findings uncover a mechanism by which nutrients and growth factors fine tune the regulation of splicing. Furthermore, our study highlights SRPK2 as a potential therapeutic target for mTORC1-driven diseases such as cancer and metabolic disorders.

Results

Identification of SRPK2 as a novel downstream target of mTORC1 signaling

We previously performed a stable isotope labeling with amino acids in cell culture (SILAC)-based quantitative phospho-proteomics screen of mTORC1 signaling and identified SRPK2 as a putative downstream target (Figure 1A) (Yu et al., 2011). The putative phosphorylation sites in SRPK2, Ser494 and Ser497, are located in the linker region that splits the kinase domain and are evolutionarily conserved among vertebrates (Figure 1B). These phosphorylation sites were also detected in mTORC1 phospho-proteomics studies carried out by other groups (Hsu et al., 2011; Robitaille et al., 2013). To verify that mTORC1 regulates phosphorylation of SRPK2, we performed SDS-PAGE mobility shift assays. Upon insulin treatment to activate mTORC1 in HEK293E cells, the mobility of SRPK2 was dramatically decreased in a time-dependent manner and the effect of insulin was completely blocked by rapamycin pretreatment (Figure 1C), indicating the presence of insulin-regulated and rapamycin-sensitive phosphorylation(s). To further characterize Ser494 and Ser497 phosphorylation, we generated phospho-specific antibodies. Consistent with the gel mobility changes, insulin induced SRPK2 phosphorylation at Ser494 and Ser497, which was abolished by rapamycin treatment or SRPK2 knockdown (Figure 1D). We also tested SPRK2 phosphorylation in cell lines that display constitutively active mTORC1 activity. In these cells, SRPK2 was phosphorylated even in the absence of growth factors, which was blunted by mTORC1 inhibition with rapamycin (Figures 1E and 1F). Together, these results indicate that SRPK2 is phosphorylated at Ser494 and Ser497 in an mTORC1-dependent manner.

S6K1 directly phosphorylates SRPK2 at Ser494 which primes for Ser497 phosphorylation by CK1

We next sought to identify the kinase(s) that directly phosphorylates SRPK2. The Ser494 residue of SRPK2 is surrounded by a phosphorylation motif (RXRXX[S/T]) recognized by the basophilic protein kinase A, G, and C (AGC) kinase family (Pearce et al., 2010a) (Figure 2A). Since S6K1 is an AGC kinase directly activated by mTORC1, we examined whether S6K1 phosphorylates SRPK2 at Ser494. Efficient knockdown of S6K1 inhibited insulin-induced phosphorylation of SRPK2 at Ser494 (Figure 2B). In addition, the S6K1 inhibitor PF4708671 (Pearce et al., 2010b) reduced SRPK2 phosphorylation as robustly as rapamycin, Torin1 (mTOR active site inhibitor) (Thoreen et al., 2009), and MK2206 (AKT inhibitor) (Yan, 2014) (Figure 2C). Expression of an activated, rapamycin-resistant form of S6K1 (F5A-T389E-R3A) (Schalm and Blenis, 2002) induced SRPK2 phosphorylation even in the presence of rapamycin (Figure 2D). To further determine whether S6K1 directly

phosphorylates SRPK2, we performed in vitro kinase assay. S6K1 immunoprecipitated from insulin treated cells, but not from rapamycin pre-treated cells, directly phosphorylated recombinant SRPK2 proteins (Figure 2E). Mutation of SRPK2-Ser494 to alanine (S494A) substantially abrogated SRPK2 phosphorylation by S6K1 (Figure 2E), demonstrating that Ser494 is the major S6K1 phosphorylation site in SRPK2. Collectively, these results indicate that S6K1 directly phosphorylates SRPK2 downstream of mTORC1 signaling.

Interestingly, we noted that Ser497 on SRPK2 is also phosphorylated in an mTORC1 and S6K1-dependent manner, and this phosphorylation is tightly correlated with phosphorylation of Ser494 (Figures 1 and 2). However, the phosphorylation motif surrounding Ser497 does not match the consensus AGC kinase substrate motif (Figure 2A). We therefore wanted to determine if the phosphorylation at Ser494 primed Ser497 for phosphorylation. We knocked down endogenous *SRPK2* with a 3' untranslated region (UTR)-targeting short-hairpin RNA (shRNA), followed by expression of SRPK2 wild-type (SRPK2-WT) or non-phosphorylatable mutants (SRPK2-S494A or S497A) in *TSC2*-deficient cells (Figures 2F and 2G). Mutation of Ser494 to alanine dramatically inhibited phosphorylation of not only Ser494 but also Ser497, whereas mutation of Ser497 to alanine affected only its own phosphorylation (Figure 2G). These data indicate that Ser494 phosphorylation is crucial for Ser497 phosphorylation. Bioinformatics analysis revealed that Ser497 becomes a casein kinase 1 (CK1) target site when Ser494 is phosphorylated (pS/TXX[S/T]) (Figure 2H) (Flotow et al., 1990). Consistent with the primed substrate recognition mechanism, CK1 directly phosphorylated the recombinant SRPK2 proteins containing a phospho-mimetic mutation at Ser494 (S494D) (Figure 2I). This phosphorylation efficiency was decreased in the non-phosphorylated S494A mutant, and even more decreased in S494A/S497A mutant (Figure 2I), suggesting that Ser497 is the primary CK1 target residue. Taken together, these results demonstrate that CK1 functions as the SRPK2-Ser497 kinase following the priming phosphorylation of Ser494 by S6K1.

Phosphorylation of SRPK2 by mTORC1 signaling is crucial for its nuclear localization

SRPK2 was shown to translocate to the nucleus and phosphorylate downstream SR proteins (Jang et al., 2009; Zhou et al., 2012). We therefore determined if insulin and mTORC1 signaling regulates nuclear-cytoplasmic shuttling of SRPK2. Endogenous SRPK2 was predominantly localized in the cytoplasm in serum-starved HEK293E cells (Figure 3A). Insulin treatment induced nuclear accumulation of SRPK2, which was blocked by Torin1 pre-treatment (Figure 3A). Consistent with the nuclear accumulation of SRPK2, phosphorylation of SR proteins was increased by insulin (Figure 3B). Notably, in cell lines with high basal mTORC1 activity, SRPK2 predominantly localized to the nucleus (Figures 3C-3E). Inhibition of mTORC1 activity by rapamycin or Torin1 (Figures 3C and 3E) or by *TSC2*-reconstitution (Figure 3D) induced cytoplasmic retention of SRPK2. These results show that insulin-mTORC1 signaling promotes nuclear localization of SRPK2.

We next investigated whether phosphorylation of SRPK2 at Ser494 and Ser497 is important for nuclear trafficking of SRPK2. In *TSC2*-deficient cells lacking endogenous *SRPK2* by knockdown (Figure 2F), exogenously expressed SRPK2-WT was localized in the nucleus (Figures 3F and 3G), whereas significantly less was observed to localize in the nucleus

following rapamycin treatment (Figures 3F and 3G). In contrast, unlike SRPK2-WT, which accumulated in the nucleus of *TSC2*-deficient cells due to its constitutive phosphorylation, the non-phosphorylatable SRPK2-S494A, S497A, and S494A/S497A mutants were distributed to the cytoplasm and this localization was not further changed by rapamycin (Figures 3F, 3G, S1A and S1B). Using in silico search, we found that SRPK2 contains a putative Importin alpha/beta-dependent nuclear-localization signal (NLS) near the Ser494 and Ser497 phosphorylation sites (Figure S1C) (Kosugi et al., 2009). Indeed, knockdown of *Importin-beta* prevented nuclear accumulation of SRPK2 (Figures S1D and S1E), suggesting that SRPK2 phosphorylation is important for Importin alpha/beta-dependent NLS recognition and nuclear translocation (Nardozzi et al., 2010). Consistently, SRPK2-WT led to increased phosphorylation of SR proteins in *TSC2*-deficient cells (Figures 3H and 3I), whereas the kinase dead (K110M) or non-phosphorylatable (S494A) SRPK2 mutant had no effect (Figures 3H and 3I). Collectively, these results demonstrate that mTORC1-dependent SRPK2 phosphorylation induces SRPK2 nuclear localization and SR protein phosphorylation.

SRPK2 regulates expression of lipid biosynthetic enzymes

SR proteins are implicated in many aspects of mRNA biogenesis such as transcription, splicing, export, translation, and stability (Chen and Manley, 2009; Fu and Ares, 2014). We therefore wanted to determine whether mTORC1-mediated regulation of SRPK2 alters RNA metabolism. To this end, we conducted whole transcriptome microarray analyses of gene expression and exon/intron utilization on *TSC2*-deficient cells after rapamycin treatment or *SRPK2* knockdown (Figure S2A). Rapamycin affected mRNA levels of 842 genes (386 increased and 456 decreased) and splice isoforms of 3,590 genes. Knockdown of *SRPK2* changed mRNA levels of 471 genes (275 increased and 196 decreased) and splice isoforms of 3,809 genes (Figures 4A, S2B and S2C). A fraction of genes (42 increased and 21 decreased) and splice isoforms (552 genes) were commonly changed by rapamycin treatment and *SRPK2* knockdown (Figure 4A).

Strikingly, among these 21 commonly decreased genes in both conditions, several encode enzymes crucial for lipid metabolism (highlighted in blue, Figure 4B) including those involved in de novo lipid synthesis such as *ACLY*, *ACSS2*, *HMGCS1*, *MVD*, and *FDFT1* (highlighted in red, Figure 4C). Quantitative real-time PCR (qPCR) confirmed that the mRNA levels of these genes were significantly suppressed by mTORC1 inhibition using rapamycin or Torin1 treatment as well as by *SRPK2* knockdown (Figure 4D). Furthermore, expression of FASN and SCD1, key enzymes for fatty acid synthesis previously linked to mTORC1 signaling (Figure 4C) (Duvel et al., 2010; Peterson et al., 2011), was also substantially decreased by *SRPK2* knockdown (Figure S2D). Consistent with the decreased mRNA expression, protein levels of these enzymes were dramatically reduced by rapamycin as well as by *SRPK2* knockdown and knockout (Figures 4E and 4F). Overexpression of wild-type SRPK2, but not the non-phosphorylatable SRPK2 mutant, restored the expression of lipogenic enzymes in *SRPK2* knockdown cells (Figure 4G). Collectively, these results show that mTORC1-SRPK2 signaling regulates a broad gene expression program linked to lipid biosynthesis.

Lipogenic genes are transcriptionally regulated by SREBP1/2 transcription factors, which are regulated by mTORC1 (Horton et al., 2002; Caron et al., 2015). Thus, we determined if SRPK2 induces lipid biosynthetic enzymes through SREBP1/2 in *TSC2*-deficient cells. In these cells, mTORC1 signaling is constitutively active independent of growth factors (Duvel et al., 2010; Zhang et al., 2014). Analysis of promoter regions covering 1 kb upstream of lipogenic genes (including SREBP-binding sites) showed that lipid deprivation by serum removal dramatically increased their promoter activity, which was suppressed by *SREBP1/2* knockdown (Figure 5A) (Horton et al., 2002). Surprisingly, despite remarkable reduction of mRNA and protein levels of lipogenic enzymes by *SRPK2* knockdown (Figure 4), we found no reduction in the promoter activity of these genes following *SRPK2* knockdown (Figure 5B). Indeed, *SCD1* and *ACSS2* displayed increased promoter activity which may reflect a feedback loop (Figure 5B). In addition, the cleavage and nuclear translocation of SREBP1, which are key steps of SREBP1 activation (Horton et al., 2002), were induced by lipid deprivation but not affected by *SRPK2* deficiency (Figure 5C). Together, these results strongly suggest that SRPK2 controls expression of target genes by post-transcriptional mechanisms.

SRPK2 increases mRNA stability of lipogenic genes by promoting efficient intron splicing

We therefore investigated whether SRPK2 regulates expression of target genes via mRNA stability. We treated cells with actinomycin D to block transcription and measured the time-dependent turnover of lipogenic mRNAs (Tani and Akimitsu, 2012). The mRNA stability of *FDFT1*, *SCD1*, *ACLY*, *ACSS2*, *HMGCS1*, and *MVD* was markedly decreased by *SRPK2* knockdown as well as by rapamycin treatment (Figure 5D). However, rapamycin or *SRPK2* knockdown did not affect the mRNA stability of *phosphofructokinase, platelet* (*PFKP*) or *ribose 5-phosphate isomerase A* (*RPIA*) (Figure 5D), known mTORC1 transcriptional target genes in glycolysis and pentose phosphate pathway, respectively (Duvel et al., 2010). Importantly, the transcriptome array analysis showed that lipogenic genes including *ACSS2*, *FDFT1*, *HMGCS1*, and *MVD* retained introns upon rapamycin treatment or *SRPK2* knockdown (Figures S3A and S3B), indicating a reduced efficiency of intron splicing. In contrast, *PFKP* or *RPIA* did not exhibit consistent intron retention under these same conditions. Introns often contain stop codons, causing ribosome stalling and recruitment of the nonsense-mediated decay (NMD) machinery, and thereby triggering degradation of abnormal mRNAs (Chang et al., 2007; Isken and Maquat, 2008). The retained introns in these genes contained stop codons (Figure S3A), suggesting that NMD could contribute to the mRNA instability by *SRPK2* deficiency. To test this possibility, we inhibited NMD by knocking down a key NMD factor, *up-frameshift 1* (*UPF1*) (Chang et al., 2007), which restored the mRNA levels of lipogenic genes in *SRPK2* knockout cells to the levels in control cells (Figures 5E and S3C). Thus, NMD, at least in part, contributes to SRPK2-controlled regulation of mRNA stability.

Since SRPK2 downstream targets, the SR proteins, are RNA binding proteins, we determined if SR proteins are involved in the regulation of lipogenic gene expression. Knockdown of some (*SRSF1/2/3*) but not all SR proteins resulted in a dramatic reduction in mRNA levels of lipogenic genes (Figures 5F and S3D), suggesting that a subset of SR proteins mediate the SRPK2-dependent regulation of lipogenic gene expression. In silico

analysis predicted several SRSF1/2/3 binding sites in lipogenic genes (Table S1). Thus, we performed RNA-immunoprecipitation assay of SRSF1 and found that lipogenic transcripts bind to SRSF1 (Figures S3E and S3F). SR proteins do not contain enzymatic activities but rather participate in the recruitment of spliceosome complex proteins (e.g., small nuclear ribonucleoproteins) to induce splicing (Kohtz et al., 1994; Lee and Rio, 2015). To test if mTORC1-SRPK2 signaling controls the interaction of SR proteins with spliceosomal proteins, we performed a proteomics-based interactome analysis for SRSF1 under vehicle vs. Torin1-treated conditions (Figure S4A). In Torin1-treated cells, we found reduced binding of SRSF1 with a small nuclear ribonucleoprotein U1 subunit 70 (SNRNP70/ U1-70k) (Figure S4B and Table S1), a spliceosomal component required for splice site recognition and subsequent assembly of the spliceosome (Lee and Rio, 2015). Co-immunoprecipitation and immunoblotting confirmed that Torin1 significantly inhibited the binding of SRSF1 with U1–70k, which was accompanied with reduced SRSF1 phosphorylation (Figure 5G). Although not previously known to be regulated by the mTORC1 pathway, phosphorylation of SRSF1 by SRPK2 was shown to promote its interaction with U1-70k, thereby enhancing splicing of pre-mRNAs (Cho et al., 2011; Kohtz et al., 1994; Wang et al., 1998). Thus, our findings are consistent with these observations and further suggest a role for mTORC1 in regulating this interaction. Finally, knockdown of *U1-70k* increased intron retention and decreased expression of several lipogenic genes, but not *PFKP* or *RPIA* (Figures 5H and S3G). Together, these results suggest that mTORC1 signaling promotes the interaction of SR proteins with the spliceosomal protein U1-70k to induce efficient splicing of lipogenic pre-mRNAs.

SRPK2 is necessary for de novo synthesis of cellular fatty acids and cholesterol

We next examined if the altered expression of lipid biosynthetic enzymes affects cellular lipid metabolism. To measure de novo lipid synthesis, we cultured *TSC2*-deficient cells in serum-free conditions with ^{14}C-labeled acetate and quantified the amount of newly synthesized fatty acids and cholesterol by HPLC (Figure 6A). Knockdown of *SREBP1/2*, as a positive control, decreased fatty acid and cholesterol synthesis (Figures S5A–S5C) (Duvel et al., 2010; Ricoult et al., 2016). Both stable and transient knockdown of *SRPK2* significantly reduced fatty acid and cholesterol synthesis (Figures 6A-6D) as did treatment with rapamycin or Torin1 (Figures 6E and 6F) (Duvel et al., 2010; Ricoult et al., 2016). We also measured de novo fatty acid synthesis in cells cultured with ^{13}C-glucose by LC-MS (Kamphorst et al., 2013). This approach allows us to determine production of different fatty acid products. In serum-free conditions, we observed only a small effect on ^{13}C incorporation into the saturated fatty acids palmitate or stearate (Figures 6G and 6H). We did, however, observe a pronounced reduction in the synthesis of oleate, which is made from stearate by desaturation (Figures 6G and 6H). Under more physiological conditions, including the presence of serum, we observed a more substantial reduction in synthesis of both saturated and especially unsaturated fatty acids from glucose (Figures 6H-6J). Altogether, these results support the important role of mTORC1-SRPK2 signaling in regulating de novo lipid synthesis.

Inhibition of SRPK2 blunts cell growth upon lipid starvation

Consistent with the reduced lipogenic potential, *SRPK2*-knocked down *TSC2*-deficient cells showed retarded cell proliferation (Figures 7A and 7B), which was more prominent when the growth was made more dependent on de novo lipid synthesis upon removal of lipids from the media (Figures 7A and 7B). Importantly, supplementation with lipoproteins (composed of cholesterol and fatty acids) or oleate (fatty acid) partially restored the growth of *SRPK2*-deficient cells (Figures 7C and 7D), indicating that the growth defect by *SRPK2* knockdown is in part due to an insufficient supply of lipids. To further validate the roles of SRPK2 on lipogenesis and cell growth, we employed an SRPK1/2 inhibitor, SRPIN340 (Fukuhara et al., 2006). SRPIN340 treatment reduced expression of lipogenic enzymes in a dose-dependent manner (Figures S6A–S6D). This inhibitory effect of SRPIN340 is likely due to SRPK2 suppression because SRPIN340 did not further reduce lipogenic gene expression in *SRPK2* knockout cells (Figure 7E). In addition, knockdown of *SRPK1*, a paralog of *SRPK2* (Wang et al., 1998), alone did not significantly affect lipogenic enzyme levels except SCD1 (Figure 7F). SRPIN340 treatment also dramatically suppressed de novo synthesis of fatty acids (Figure S6E) and cell growth in tumor cell lines with high mTORC1 activity (Figures 7G and S6F). To test the in vivo relevance of these findings in the context of cancer, we conducted xenograft growth studies with cell lines with high mTORC1 activity. Strikingly, both genetic (knockdown or knockout) and pharmacological inhibition of SRPK2 inhibited tumor growth across each of these multiple cancer cell line xenograft models (Figures 7H-7K, S6G and S6H). Thus, these results further demonstrate that SRPK2 is a crucial downstream mediator for mTORC1-dependent lipogenesis, a process that contribute substantially to tumor growth.

Discussion

Here we report an unexpected link between the mTORC1 and SRPK2 signaling pathways. This signaling axis seems to be a key post-transcriptional regulator of lipid biosynthetic enzymes to support cell proliferation. Together with the known stimulatory function of mTORC1 on SREBP-dependent transcription, our study reveals that mTORC1 signaling utilizes both transcriptional and post-transcriptional mechanisms to amplify cellular lipid biogenesis (Figure S7).

Our findings indicate that the functional consequence of SRPK2 phosphorylation by mTORC1/S6K1 is its translocation from cytoplasm to nucleus (Figure 3). The downstream substrates of SRPKs, SR proteins, are involved in RNA metabolism and predominantly locate in the nucleus (Fu and Ares, 2014; Ghosh and Adams, 2011). Accordingly, SRPK2 nuclear localization is a critical node by which upstream signals (e.g. mTORC1/S6K1) regulate SRPK2 signaling. Previously, AKT was shown to induce SRPK2 phosphorylation at Thr492 to enhance its binding to 14-3-3 proteins (which often retain associated proteins in the cytoplasm) (Jang et al., 2009; Rittinger et al., 1999). However, AKT activation paradoxically resulted in SRPK2 nuclear accumulation (Jang et al., 2009). Since AKT activates mTORC1/S6K1 signaling, SRPK2 nuclear localization downstream of AKT is consistent with our results (Figure 3). It is possible that AKT temporally retains SRPK2 in the cytoplasm via 14-3-3 proteins, but S6K1 activation downstream of AKT subsequently

induces SRPK2 nuclear translocation not only via SRPK2 phosphorylation but possibly also via AKT inhibition through the well-established negative feedback mechanisms regulated by mTORC1 and S6K1 (Mendoza et al., 2011).

Another interesting aspect of SRPK2 phosphorylation is that the Ser494 phosphorylation by mTORC1/S6K1 induces subsequent Ser497 phosphorylation by CK1 (Figure 2). Although CK1 is constitutively active, its action on substrates is usually contingent upon priming phosphorylation by a different kinase (Flotow et al., 1990; Cheong and Virshup, 2011). For example, phosphorylation of DEPTOR on Ser293 and Ser299 by mTORC1 is followed by CK1, which creates a binding site on DEPTOR for βTrCP ubiquitin ligase (Duan et al., 2011; Gao et al., 2011). The amino acids around the SRPK2 phosphorylation sites are an Importin-alpha/beta-dependent NLS sequence (Figure S1C) (Kosugi et al., 2009), whose interaction with substrates is known to be enhanced by substrate phosphorylation around the NLS (Nardozzi et al., 2010). Thus, sequential phosphorylation by mTORC1/S6K1 and CK1 promotes efficient nuclear accumulation of SRPK2 and downstream signaling. It will be of great interest to investigate the kinetics of SRPK2 nuclear localization and how this results in additional nuclear phosphorylation events and mTORC1-dependent interaction with other proteins.

To support increased proliferation rates, cancer cells rewire their metabolism to meet the high demand for biosynthesis of macromolecules. Targeting metabolism has recently emerged as a new therapeutic strategy for cancer treatment (DeBerardinis and Thompson, 2012; Vander Heiden et al., 2009). Expression of enzymes for lipid biosynthesis such as *ACLY*, *ACC*, *FASN*, and *SCD1* is often elevated in tumors (Currie et al., 2013; Menendez and Lupu, 2007). Indeed, inhibition of these enzymes has been reported in certain cases to selectively kill cancer cells and retard tumor growth in xenograft models (Currie et al., 2013; Menendez and Lupu, 2007). SRPK2 is overexpressed in several cancer types including lung, colon, and acute myeloid leukemia (Gout et al., 2012; Jang et al., 2008; Wang et al., 2016). SRPK2 is a kinase, and therefore, a promising druggable target (Cohen, 2002; Fukuhara et al., 2006; Zhang et al., 2009). It is thus plausible to develop compounds that specifically inhibit SRPK2 for clinical use. Our results showed that SRPK2 inhibition with lipid deprivation inhibits cancer cell proliferation (Figure 7). Therefore, combination therapies using specific SRPK2 inhibitors and lipid uptake blockers such as CD36 antibodies (Pascual et al., 2016; Selwan et al., 2016) would also be a promising regimen for treatment of cancers with high dependency on mTORC1 signaling and lipid metabolism.

STAR Methods

CONTACT FOR REAGENT AND RESOURCE SHARING

Further information and requests for resources and reagents should be directed to and will be fulfilled by the Lead Contact, John Blenis (job2064@med.cornell.edu).

EXPERIMENTAL MODEL AND SUBJECT DETAILS

Cell lines—RT4, MCF7, DLD1, A549, and mAb104 cells were obtained from ATCC. HEK293T cells were obtained from GenHunter. Human renal angiomyolipoma-derived

LAM 621-101 (*TSC2*–/–) cell line immortalized by HPV E6/E7 and hTERT was described before (Yu et al., 2004). Eker rat uterine leiomyoma-derived ELT3 (*Tsc2*–/–) cell line was provided by Cheryl Walker (Texas A & M University) (Howe et al., 1995) and used to generate ELT3-luciferase cell line stably expressing luciferase as previously described (Yu et al., 2009). *Tsc2*–/– mouse embryonic fibroblasts (MEFs) were provided by David Kwiatkowski (Harvard Medical School) (Zhang et al., 2003). Cells were grown in the following media at 37°C with 5% CO_2 unless otherwise stated. HEK293E, HEK293T, RT4, and *Tsc2*–/– MEFs were cultured in DMEM with 10% FBS. MCF7, DLD1, and A549 cells were cultured in RPMI with 10% FBS. mAb104 cells were cultured in Iscove's modified Dulbecco's medium (IMDM) with 20% FBS. LAM 621-101 and ELT3 cells were cultured in IIA complete media (DMEM/F12, 10% FBS, 1 nM triiodothyronine, 10 μU/mL vasopressin, 200 nM hydrocortisone, 50 nM sodium selenite, 10 nM cholesterol, 20 ng/mL EGF, 25 μg/mL insulin, 10 μg/mL transferrin, and 1.6 μM ferrous sulfate) (Yu et al., 2004; Yu et al., 2009).

Mice—All animal work was performed in accordance with protocols approved by the University of Cincinnati Standing Committees on Animals. 6–8 week-old female nude CD-1 mice (Charles River), NOD/SCID-gamma mice (Jackson Lab), and CB17-scid mice (Taconic) were used.

Microbe strains—*E. coli* BL21 (New England Biolabs) was grown at 28°C in 2x YTA medium for protein purification.

METHODS DETAILS

Antibodies and small molecule inhibitors—Cell Signaling Technology custom developed the pSRPK2(S494), pSRPK2(S497), and pSRPK2(S494/S497) antibodies for this study. Antibodies were obtained from following sources: SRPK1 and SRPK2 from BD Biosciences; ACLY, FASN, SCD1, S6, pS6(S235/S236), pS6(S240/S244), S6K1, pS6K1(T389), TSC2, and V5 from Cell Signaling Technology; ACSS2 and GAPDH from Sigma-Aldrich; FDFT1 from Abcam; SRSF1, ACTIN, GST, LAMIN A/C, and SREBP1 from Santa Cruz; HA from Covance; U1-70k from Synaptic Systems. Monoclonal antibody for the phosphorylated SR proteins was generated from the mAb104 hybridoma cell line (ATCC) (Figures 3B and 3H) or purchased from invitrogen (mAB1H4) (Figure 5G). Reagents were obtained from following sources: Insulin, rapamycin, PF4708671, and actinomycin D from Sigma-Aldrich; Torin1 from Tocris Bioscience; rapamycin from Calbiochem; MK2206 from Cayman Chemical; SRPIN340 from Selleck Chemicals and Milstein Chemistry Core Facility (Weill Cornell Medicine).

Gene expression analysis and measurement of mRNA stability—RNA was isolated using RNeasy Mini Kit (Qiagen) or PureLink RNA Mini kit (Ambion) and treated with DNase I (Qiagen or Sigma-Aldrich) according to the manufacturers' instructions. After reverse-transcription of 500-1,000 ng RNA (iScript cDNA synthesis kit, Bio-rad), the resulting cDNA was diluted in nuclease-free water (1:5) followed by quantitative real-time PCR (qPCR) using QuantStudio 6 Flex (Applied Biosystems). Gene expression levels were normalized to the expression level of the housekeeping genes *ACTIN*, *TATA-binding protein*

(*TBP*) or *Peptidylpropyl isomerase B* (*PPIB*). To measure mRNA stability, transcription was blocked by actinomycin D (5 μg/ml) treatment for 0, 2, and 4 hr. Reverse-transcription was performed using the same volume of RNA for all time points and the mRNA levels were measured by qPCR (Tani and Akimitsu, 2012).

Human whole transcriptome microarray—Total RNA was isolated using RNeasy Mini Kit (Qiagen) and treated with DNase I (Qiagen). Microarray was performed by the Translational Genomics Core at Partners HealthCare Personalized Medicine (MA, USA) according to the protocol from Affymetrix. Briefly, 100 ng total RNA was used to synthesize biotinylated cDNA using GeneChip whole transcript (WT) plus reagent kit. 5.5 μg cDNA was fragmented and labeled by terminal deoxynucleotidyl transferase (GeneChip WT terminal labeling kit). The resulting cDNA was hybridized to the Human Transcriptome 2.0 Array at 45°C for 16 hr. Array chips were washed and stai ned using GeneChip fluidics station 450, and scanned using GeneChip Scanner 3000 7G. Data were analyzed by Expression console (Affymetrix) and Transcriptome analysis console software (Affymetrix) according to the manufacturer's instruction.

HPLC analysis of de novo lipid synthesis—Cells in a 6-well plate were cultured in serum-free DMEM (5.5 mM glucose) overnight or for 24 hr (for drug treatment conditions), and labeled with $[1-{}^{14}C]$-acetate (2–8 μCi/well) (Perkin Elmer) for the last 6 hr. The cells were washed three times with PBS and lysed by methanol containing the internal standard 13(S)-hydroxyoctadecadienoic acid [13(S)-HODE] (2 μg/well) (Cayman Chemicals). Cell lysates were collected with a cell scraper and transferred to a glass vial. Lipids were extracted by addition of chloroform and water (methanol:chroloform:water = 1:1:0.9, by volume). After centrifugation (800 rpm, 10 min), the lower phase was transferred to a new vial and evaporated under a stream of N_2. The lipids were then dissolved in methanol (1 mL), hydrolyzed by 0.5 ml of 1 N NaOH at room temperature for 2 hr, and re-extracted by addition of chloroform (2 mL), 1N HCl (0.5 mL), and water (2 mL). After centrifugation, the lower phase was transferred to a new vial. Samples were evaporated under a stream of N_2 and dissolved in 0.2 mL of hexane:isopropanol:acetic acid (100:3:0.02, by volume) for HPLC analysis. Samples were analyzed using an Agilent Zorbax Silica column (5 μm, 4.6×250 mm) with isocratic elution of hexane:isopropanol:acetic acid (100:3:0.02, by volume) at a flow rate of 1 mL/min over 12 min, on an Agilent 1260 Infinity binary system with a Diode array detector coupled to a Perkin-Elmer Radiometric 150TR detector (Zheng et al., 2011). The retention time of fatty acids and cholesterol was determined by standard lipids. Peak areas of radiolabeled fatty acids and cholesterol were integrated (Agilent OpenLAB CDS ChemStation) and normalized to that of 13(S)-HODE and cell number.

LC-MS analysis of saponified fatty acids—Extraction and LC-MS analysis of fatty acids were performed as previously described (Kamphorst et al., 2013). Briefly, cells in a 60-mm plate were supplemented with 17.5 mM $[U-{}^{13}C]$-glucose (Cambridge Isotope Laboratories) in DMEM/F12 with or without 10% dialyzed FBS (Sigma-Aldrich) or lipoprotein-deficient serum (Intracel or Alfa Aesar) for 48 hr. The cells were washed three times with PBS and lysed with 2 mL of 0.3 M KOH in 90% methanol. Cell lysates were collected with a cell scraper and transferred to a glass vial. Lipids were hydrolyzed at 80°C

for 1 hr and formic acid (0.2 mL) was added for neutralization. The lipids were extracted twice by adding 2 mL of hexane and transferring the top layer to a new vial. Samples were evaporated under a stream of N_2 and dissolved in 0.1 mL of isopropanol:methanol (1:1, v/v) solution for LC-MS analysis (Stand-alone Orbitrap, Thermo Fisher). De novo synthesized fatty acids were determined based on the sum of all forms containing four or more labeled carbon atoms (fatty acids containing 2-labeled carbon atoms are made from elongation not de novo synthesis). Data analysis with MAVEN software and natural isotope correction were performed as previously described (Kamphorst et al., 2013).

Cell proliferation assay—Cells seeded on a 12-well plate (LAM 621-101, 2×10^3 cells; MCF7 and RT4, 2×10^4 cells) were grown in the media (LAM 621-101, DMEM/F12; MCF7, RPMI; RT4, DMEM) with 10% FBS or LPDS for 8 days. Lipoprotein (25 μg/ml), oleic acid-albumin (50 μM), or fatty acid-free albumin (25 μM) was supplemented to the media. Cristal violet staining was performed to visualize cells. Briefly, cells were fixed with 4% methanol-free formaldehyde (Polysciences) in PBS for 30 min and rinsed with PBS. The cells were incubated with 0.1% crystal violet solution (Sigma-Aldrich) for 30 min at room temperature. After rinsing five times with water, the plate was air-dried and scanned. Quantification was performed by densitometry analysis of images using Adobe Photoshop.

In vivo xenograft tumor assay—All animal work was performed in accordance with protocols approved by the University of Cincinnati Standing Committees on Animals. Female nude CD-1 mice (Charles River) (A549 cell line), NOD/SCID-gamma mice (Jackson Lab) (LAM 621-101 cell line), and CB17-scid mice (Taconic) (RT4 and ELT3-luciferase cell lines), 6 to 8 weeks of age, were used. 2×10^6 cells were subcutaneously inoculated into the posterior back regions of each mouse. Once the tumor is formed three to five weeks post inoculation, tumor length and width were measured using a digital caliper. Tumor volume was calculated using the formula: volume = (length × (width)^2/2). For the drug treatment experiment, mice were randomized into two groups after tumor formation and treated with either vehicle control (100 μl of 1% DMSO in PBS) or SRPIN340 (100 μl of 20 μg/ml; 1% DMSO in PBS) by daily peritumoral injection as previously described (Gammons et al., 2014). SRPIN340 was dissolved as 2 mg/ml in DMSO, and this stock solution was diluted 1:1,000 using PBS prior to inject. For the bioluminescent imaging of ELT3-luciferase tumors, luciferin (120 mg/kg, Xenogen) was intraperitoneally injected into the mouse 10 min prior to imaging. Bioluminescent signals were recorded using the Xenogen IVIS System and the total photon flux of tumors was analyzed as previously described (Yu et al., 2009).

Mass spectrometry analysis of SRSF1 interactome—HEK293E cells were transfected with empty vector (EV) or pLX304-SRSF1-V5. After 24 hr transfection, cells were treated with vehicle (DMSO) or Torin1 (250 nM) for additional 4 hr according to the three experimental conditions: EV+DMSO, SRSF1-V5+DMSO, and SRSF1-V5+Torin1. Cells were washed once with ice-cold PBS and disrupted on ice with lysis buffer (50 mM Tris-Cl buffer [pH 8], 150 mM NaCl, and 0.5% NP-40) supplemented with protease inhibitors (250 μM PMSF, 5 μg/ml pepstatin A, 10 μg/ml leupeptin, and 5 μg/ml aprotinin), phosphatase inhibitors (PhosSTOP, Roche), and RNase inhibitor (160 unit/ml). Lysates were

homogenized by syringe. Cleared lysates were obtained by centrifugation at 15,000 rpm at 4 °C for 30 min. For co-immunoprecipitation, lysates were incubated with anti-V5 agarose affinity gel (Sigma-Aldrich) at 4 °C for 2.5 hr and washed three times with the lysis buffer. Immunoprecipitated proteins were analyzed by immunoblotting or further processed for the mass spectrometry (MS) analysis.

For MS analysis, the immunoprecipitated proteins were eluted from the beads by incubating with V5 peptide (Sigma-Aldrich) overnight at 4°C. Protei n elutes were precipitated with trichloroacetic acid (TCA, 20% w/v), rinsed three times with acetone, and dried at room temperature. The pellets were re-suspended in 50 μL resuspension buffer (8 M urea, 50 mM ammonium bicarbonate, and 5 mM DTT) and subjected to reduction and alkylation reaction. Briefly, 15 mM iodoacetamide was added to each sample for 30 min in the dark at room temperature, followed by addition of another 5 mM DTT to quench the reaction. Samples were diluted to a final concentration of 1 M urea, and then subsequently digested with LysC (room temperature, overnight) and trypsin (37°C, overnight) (each at a ratio of 1:125, enzyme:protein).

Samples were then labeled using triplex reductive dimethylation (Boersema et al., 2008). Labeling was done while the peptides were bound to the solid phase C18 resin in self-packed STAGE tip micro-columns. Stage tips were washed as previously described with methanol, acetonitrile (ACN, 70% v/v) and formic acid (FA, 1% v/v), and finally with 1% FA. Samples were acidified by adding 100% FA to a final concentration of 2% FA before loading. After sample loading, stage tips were washed with 1% FA and phosphate/citrate buffer (0.23 M sodium phosphate and 86.4 mM citric acid [pH 5.5]). At this point, the "light" solution for EV+DMSO (0.4% CH_2O and 60 mM $NaBH_3CN$)', "medium" solution for SRSF1-V5+DMSO (0.4% CD_2O and 60 mM $NaBH_3CN$), or "heavy" solution for SRSF1-V5+Torin1 (0.4% $^{13}CD_2O$ and 60 mM $NaBD_3CN$) was added twice on each stage tip to label the peptides. A final wash with 1% FA was performed prior to elution with 70% ACN and 1% FA. Samples were dried under vacuum, resuspended in 5% FA, and mixed together in equal amounts for analysis using an Orbitrap Fusion Mass Spectrometer (Thermo Fisher). Peptides were introduced into the mass spectrometer by nano-electrospray as they eluted off a self-packed 40 cm, 75 μm (ID) reverse-phase column packed with 1.8 μm, 120 Å pore size, SEPAX C18 resin. Peptides were separated with a gradient of 5–25% buffer B (99.9% ACN, 0.1% FA) with a flow rate of 350 nl/min for 85 min. For each scan cycle, one high mass resolution full MS scan was acquired in the Orbitrap mass analyzer at a resolution of 120K, AGC value of 500,000, in a m/z scan range of 375-1,400, max acquisition time of 100 ms and up to 20 parent ions were chosen based on their intensity for collision induced dissociation (normalized collision energy = 35%) and MS/MS fragment ion scans at low mass resolution in the linear ion trap. Dynamic exclusion was enabled to exclude ions that had already been selected for MS/MS in the previous 40 sec. Ions with a charge of +1 and those whose charge state could not be assigned were also excluded. All scans were collected in centroid mode.

Two biological replicates for each condition were processed and analyzed. All raw mass spectral data were processed using the Maxquant analysis platform and subsequent visualization and statistical analysis was done with Perseus (Tyanova et al., 2016). Spectra

were searched using the Andromeda algorithm. Prior to run Maxquant, the following dynamic and fixed modifications were set: oxidation methionine and acetyl protein N-term (as dynamic), carbamidomethyl in cysteines (as fixed). Spectral matches were filtered to 1% false positive rate.

SILAC cell culture and mass spectrometry analysis of phosphorylated proteins—Sample preparation for the stable isotope labeling with amino acids in cell culture (SILAC) experiments and LC-MS/MS analysis were previously described (Yu et al., 2011). Briefly, *Tsc2*–/–MEFs were grown in light ($[^{12}C_6{}^{14}N_2]$-Lys, $[^{12}C_6{}^{14}N_4]$-Arg) or heavy ($[^{13}C_6{}^{15}N_2]$-Lys, $[^{13}C_6{}^{15}N_4]$-Arg) (Cambridge Isotope Laboratories) DMEM supplemented with 10% dialyzed FBS. Cells were serum starved for 17 hr and treated with vehicle or rapamycin (20 nM) for 2 hr. Cells were lysed and digested with trypsin, and the phospho-peptides were enriched by SCX-IMAC method. Samples were analyzed by LTQ-Orbitrap mass spectrometer (Thermo Fisher) as previously described (Yu et al., 2011).

RNA-protein immunoprecipitation (RNA-IP)—RNA-protein immunoprecipitation was performed using Imprint RNA immunoprepitation (RIP) kit (Sigma-Aldrich) according to the manufacturer's protocol. Cells on a 15-cm plate were washed twice with ice-cold PBS and harvested into Eppendorf tube. Cells were collected by centrifugation at 3,000 rpm at 4 °C for 5 min. Cell pellets were re-su spended with 100 μL of strong lysis buffer (RIP kit) supplemented with protease inhibitors (protease inhibitor cocktail, 1 μL) and RNase inhibitor (160 unit/mL) and incubated on ice for 15 min. Cell lysates were snap-frozen in liquid nitrogen and thawed on ice.

To prepare antibody-prebound beads, 5 μg of mouse IgG (EMD Millipore) or anti-SRSF1 antibody (Santa Cruz) was conjugated to the 50 μL protein A/G magnetic beads (Thermo Fisher). Cell lysates and the antibody-prebound beads were incubated in 1 mL RIP buffer at 4 °C for 3 hr. Beads were washed and RNA was eluted by incubating with 150 μL RIP buffer containing 1% SDS and 1.2 mg/mL proteinase K (New England Biolabs) at 55°C fo r 30 min. The eluted RNA was further purified by phenonol/chroloform extraction and precipitated with ammonium acetate and ethanol. Input and immunoprecipitated RNAs were treated with DNase I (Sigma-Aldrich) and reverse-transcribed (iScript cDNA synthesis kit, Bio-rad), and the resulting cDNA was analyzed by qPCR as described in the Gene expression analysis section. The amount of transcripts (%) bound to the antibody was calculated: $100 \times 2^{[Ct(input) - Ct(IP)]}$.

Luciferase promoter activity assay—Cells plated on a 6-well plate were co-transfected with 1 μg of renillia construct containing the promoter of interested gene and 0.2 μg of control cypridina construct using FuGENE HD transfection reagent (Promega). For co-transfection of luciferase constructs with siRNA, SE Cell Line 4D-Nucleofector X Kit and 4D-Nucleofector system (Lonza) were used. 48 hr after transfection, the activity of luciferase was measured by LightSwitch dual assay system (SwitchGear Genomics) according to the manufacturer's protocol. Renilla luciferase activity was normalized by cypridina luciferase activity.

Expression constructs and mutagenesis—For expression studies, the coding sequence of human *SRPK2* (NM_001278273.1) was cloned into pKH3 vector (BclI/BamHI and MfeI/EcoRI), and the HA-SRPK2 from pKH3-SRPK2 was subcloned into pLNCX vector (NotI and SalI). To generate GST-tagged SRPK2 protein for in vitro kinase assays, 454-521 amino acids of SRPK2 was cloned into pGEX-2T vector (EcoRI). pLX304-SRSF1-V5 and pCMV-SPORT6-mouse Srpk2 were obtained from Harvard PlasmID. To generate pLenti-Blast-mouse Srpk2, pCMV-SPORT6-Srpk2 was recombined with pDONR223 vector by BP reaction (Gateway BP clonase II enzyme mix, Invitrogen), and the resulting pDONR223-Srpk2 was recombined with pLenti-Blast-DEST vector by LR reaction (Gateway LR clonase II enzyme mix, Invitrogen). SRPK2 mutants (S494A, S494D, S497A, S494A/S497A, and K110M for human SRPK2; S488A/S491A for mouse Srpk2) were generated using QuickChange site-directed mutagenesis kit (Strategene). The constitutively active S6K1 construct (pKH3-S6K1-F5A/T389E/R3A) was previously described (Schalm and Blenis, 2002).

siRNA and shRNA expression—Pooled siRNAs (30 nM) were transfected using Lipofectamine RNAiMAX reagent. For the rescue experiment in Figure 4G, 10nM of siRNA targeting 3' UTR of *SRPK2* (SASI_Hs01_00057789) was used. pLKO.1 shRNA constructs were from the RNAi Consortium (TRC) at the Broad Institute: shGFP (TRCN0000072181), shSRPK2#6 (TRCN0000006274, targeting 3' UTR), and shSRPK2#10 (TRCN0000006278, targeting CDS). Results from shSRPK2#6 are shown as representative data unless otherwise stated.

CRISPR/Cas9 knockout—Each guide RNA sequence targeting human *SRPK2* (GCATTATACGGAGACAGCCT, GGATCCGCGGAATGCAGATA, and GACGCGTCAGTACCGCTCCA) was cloned into lentiCRISPRv2 vector (Sanjana et al., 2014). LAM 621-101 cells were infected with viral supernatants generated from lentiCRISPRv2 and selected with puromycin (10 μg/mL). Single cell cloning was performed by serial dilution in 96-well plates, followed by immunoblot analysis of SRPK2 to confirm knockout efficiency of multiple selected clones. Immunoblot result of the *SRPK2* knockout cells generated from the guide RNA, GCATTATACGGAGACAGCCT, is shown.

Generation of stable cell lines—HEK293T cells were co-transfected with the viral plasmid of interest with packaging and envelope plasmids according to the viral vectors (pLKO.1, pLenti-Blast and lentiCRISPRv2, lentiviral; pLNCX, retroviral) using Lipofectamine 2000 reagent as previously described (Csibi et al., 2014). Virus-containing supernatants were collected at 48 hr after transfection. Target cells were infected with 0.45 μM-filtered viral supernatant in the presence of 8 μg/mL polybrene for 24 hr. pLKO.1 or lentiCRISPRv2-infected LAM 621-101 cells were selected with 10 μg/mL puromycin. pLKO.1-infected A549 cells were selected with 2 μg/mL puromycin. pLenti-Blast-infected LAM 621-101 cells were selected with 30 μg/mL blasticidin. LAM 621-101 cells stably expressing empty vector or *TSC2* were provided by Elisabeth Henske (Siroky et al., 2012).

Cell lysis, fractionation, immunoprecipitation, and immunoblotting—Cells were washed twice with ice-cold PBS and homogenized on ice either in a regular lysis buffer (40

mM HEPES [pH 7.4], 1 mM EDTA, 120 mM NaCl, 0.5 mM DTT, 10 mM β-glycerophosphate, 1 mM NaF, 1 mM Na_3VO_4, 0.1% Brij-35, 0.1% deoxycholate, and 0.5% NP-40) or in a Triton X-100 lysis buffer (40 mM HEPES [pH 7.4], 1 mM EDTA, 120 mM NaCl, 0.5 mM DTT, 10 mM β-glycerophosphate, 1 mM NaF, 1 mM Na_3VO_4, and 1% Triton X-100) supplemented with protease inhibitors (250 μM PMSF, 5 μg/ml pepstatin A, 10 μg/ml leupeptin, and 5 μg/ml aprotinin). Cell lysates were cleared by centrifugation at 13,000 rpm at 4 °C for 20 min. Isolation of nuclear vs. cytoplasmic fractions was performed using an NE-PER kit (Thermo Fisher Scientific) according to the manufacturer's protocol. Protein concentration was measured by Bradford assay (Bio-rad) and the proteins were denatured by boiling for 10 min in a sample buffer. 15–30 μg of proteins were analyzed by immunoblotting as previously described (Csibi et al., 2014). Immunoblot signals were detected by Odyssey imaging system (LI-COR Biosciences) or enhanced chemiluminescence (ECL), and quantified by densitometry analysis of protein bands using Adobe Photoshop or Odyssey imaging system. Immunoblot images are representative of at least two independent experiments. Numbers below the immunoblot bands indicate the average band intensity of two representative immunoblot images normalized to the loading control.

For calf intestinal alkaline phosphatase (CIAP, New England Biolabs) treatment, cells were lysed in a CIAP buffer (New England Biolabs) supplemented with 1% Triton X-100, 1 mM DTT, and protease inhibitors. 50 μg of cell lysates were treated with 50 unit of CIAP at 37°C for 1 hr.

For immunoprecipitation of HA-S6K1, cells were lysed using a Triton X-100 lysis buffer (without DTT). 1 mg of cell lysates were incubated with primary antibodies at 4 °C for 4 hr, followed by incubation with 50% slurry of protein A/G sepharose beads (GE Healthcare Life Sciences) presaturated with lysis buffer for additional 1 hr. After rinsing three times with the lysis buffer, the immunoprecipitated proteins were used for further analysis.

Protein purification and in vitro kinase assays—For GST-SRPK2 protein purification, *E. coli* BL21 (New England Biolabs) was transformed with pGEX-2T-SRPK2 plasmids. The bacteria were grown at 28°C in 2x YTA medium containing 100 ug/ml ampicillin until A_{600} of 0.6–0.8, followed by 100 nM IPTG treatment for 2 hr to induce protein expression. The cells were harvested by centrifugation at 6,000 g at 4°C for 15 min and re-suspended in ice-cold PBS. The cells were lysed with sonicator, followed by incubation with 1% Triton X-100 at 4°C for 30 min. Cell lysates were c leared by centrifugation at 12,000 g at 4°C for 10 min and incubated with 50% slurry of Glutathione Sepharose 4B (GE Healthcare Life Sciences) at 4°C for 2 hr. After rinsing three times with PBS, p roteins were eluted with 1 mL elution buffer (50 mM Tris-HCl and 10 mM reduced glutathione, pH 8.0).

For S6K1 in vitro kinase assay, immunoprecipitated HA-S6K1 from HEK293E was incubated with 1 μg of GST-SRPK2 in a kinase assay buffer (25 mM Tris-HCl, [pH 7.4], 10 mM $MgCl_2$, 5 mM β-glycerophosphate, 2 mM DTT, and 100 μM ATP) containing 5 μCi [γ-^{32}P]-ATP (Perkin Elmer) at 30°C for 20 min. For CK1 in vitro kinase assay, 200 ng of GST-CK1 (EMD Millipore) was incubated with GST-SRPK2 in the kinase assay buffer

containing 5 µ [γ-^{32}P]-ATP at 30°C for 30 min. Samples were separated by SDS-PAGE, blotted onto nitrocellulose membrane, and subjected to autoradiography.

Immunofluorescence staining—Cells grown on a fibronectin and gelatin-coated glass coverslip in a 12-well plate were fixed with 4% methanol-free formaldehyde in PBS for 30 min. The cells were rinsed with PBS and permeabilized with 0.1% Triton X-100 in PBS for 10 min. Then the cells were blocked for 1 hr with the blocking buffer (50:50 mixture of 0.1% Triton X-100 buffer and LI-COR blocking buffer, LI-COR Biosciences) and incubated with anti-SRPK2 (1:100 dilution, BD Biosciences) and anti-pS6(S235/S236) (1:200 dilution, Cell Signaling Technology) antibodies in the blocking buffer overnight at 4°C. After rinsing three times with the Triton X-100 buffer, cells were incubated with the secondary antibodies conjugated with Alexa488 or with Alexa568 (1:1,000 dilution in the blocking buffer) at room temperature for 1 hr and washed three times with the Triton X-100 buffer. The cells were then incubated with 0.5 ug/mL Hoechst 33258 (Thermo Fisher) in PBS for 10 min, rinsed twice with PBS, and mounted onto the glass slides with a Dako mounting medium (Sigma-Aldrich). Images were taken using Nikon upright microscope or Zeiss laser scanning confocal microscope, and analyzed using MetaMorph software at Nikon Imaging Center (Harvard Medical School). For the quantification of cell numbers regarding nuclear-cytoplasmic localization of SRPK2, the average intensity of nuclear-SRPK2 (nucleus area is determined as overlapping with DAPI signal) was measured in control cells, and the cells containing nuclear-SRPK2 intensity above the average intensity of control were counted as nucleus.

Bioinformatics and in silico analysis—For the gene ontology (GO) enrichment analysis (Figure S2C and Table S2D), the list of genes was uploaded to the DAVID database website (http://david.abcc.ncifcrf.gov) for biological pathway analysis. The criteria selected for the analysis were: gene identifier (OFFICIAL_GENE_SYMBOL), background genes (whole human genome), and analytic tool (functional annotation).

For the transcription factor enrichment analysis (Figure S2D), the list of genes was uploaded to the web-based gene set analysis toolkit (http://www.webgestalt.org) for identification of transcription factor binding site enrichments in upstream promoter regions. The criteria selected for the analysis were: organism (hsapiens), method (overrepresentation enrichment analysis, ORA), functional database (network, Transcription_factor_target), gene ID type (genesymbol), and reference set for enrichment analysis (affy_hta_2_0).

To analyze putative SRSF1, SRSF2, and SRSF3 binding sites (Table S1), the mRNA sequence of the transcripts was uploaded to the web server for mapping binding sites of RNA-binding proteins (http://rbpmap.technion.ac.il) (Paz et al., 2014). The criteria selected for the analysis were: RNA binding protein (Human/mouse motifs; SRSF1, SRSF2, and SRSF3) and Stringency level (high stringency).

STATISTICAL ANALYSIS

Data obtained from the qPCR, immunoblot, immunofluorescence staining, crystal violet staining, HPLC, and proteomics were statistically analyzed using Student's t test and the graphs show mean ± SD. Data obtained from the whole transcriptome array and tumor

xenograft assays were statistically analyzed using ANOVA analysis and the graphs show mean ± SEM. Detailed methods and p value for the statistical significance are described in the figure legends and methods details.

DATA AVAILABILITY

The whole transcriptome microarray data have been deposited in NCBI's Gene Expression Omnibus and are accessible through GEO Series accession number GSE104335 (https://www.ncbi.nlm.nih.gov/geo/query/acc.cgi?acc=GSE104335).

Supplementary Material

Refer to Web version on PubMed Central for supplementary material.

Acknowledgments

References

Boersema PJ, Aye TT, van Veen TAB, Heck AJR, Mohammed S. Triplex protein quantification based on stable isotope labeling by peptide dimethylation applied to cell and tissue lysates. Proteomics. 2008; 8:4624–4632. [PubMed: 18850632]

Caron A, Richard D, Laplante M. The Roles of mTOR Complexes in Lipid Metabolism. Annu. Rev. Nutr. 2015; 35:321–348. [PubMed: 26185979]

Chang Y-F, Imam JS, Wilkinson MF. The nonsense-mediated decay RNA surveillance pathway. Annu. Rev. Biochem. 2007; 76:51–74. [PubMed: 17352659]

Chen M, Manley JL. Mechanisms of alternative splicing regulation: insights from molecular and genomics approaches. Nat. Rev. Mol. Cell Biol. 2009; 10:741–754. [PubMed: 19773805]

Cheong JK, Virshup DM. Casein kinase 1: Complexity in the family. Int. J. Biochem. Cell Biol. 2011; 43:465–469. [PubMed: 21145983]

Cho S, Hoang A, Sinha R, Zhong X-Y, Fu X-D, Krainer AR, Ghosh G. Interaction between the RNA binding domains of Ser-Arg splicing factor 1 and U1-70K snRNP protein determines early spliceosome assembly. Proc. Natl. Acad. Sci. U. S. A. 2011; 108:8233–8238. [PubMed: 21536904]

Cohen P. Protein kinases — the major drug targets of the twenty-first century? Nat. Rev. Drug Discov. 2002; 1:309–315. [PubMed: 12120282]

Crino PB, Nathanson KL, Henske EP. The tuberous sclerosis complex. N. Engl. J. Med. 2006; 355:1345–1356. [PubMed: 17005952]

Csibi A, Lee G, Yoon S-O, Tong H, Ilter D, Elia I, Fendt S-M, Roberts TM, Blenis J. The mTORC1/S6K1 pathway regulates glutamine metabolism through the eIF4B–dependent control of c-Myc translation. Curr. Biol. 2014; 24:2274–2280. [PubMed: 25220053]

Currie E, Schulze A, Zechner R, Walther TC, Farese RV. Cellular fatty acid metabolism and cancer. Cell Metab. 2013; 18:153–161. [PubMed: 23791484]

DeBerardinis RJ, Thompson CB. Cellular metabolism and disease: what do metabolic outliers teach us? Cell. 2012; 148:1132–1144. [PubMed: 22424225]

Dibble CC, Manning BD. Signal integration by mTORC1 coordinates nutrient input with biosynthetic output. Nat. Cell Biol. 2013; 15:555–564. [PubMed: 23728461]

Duan S, Skaar JR, Kuchay S, Toschi A, Kanarek N, Ben-Neriah Y, Pagano M. mTOR Generates an Auto-Amplification Loop by Triggering the βTrCP- and CK1α-Dependent Degradation of DEPTOR. Mol. Cell. 2011; 44:317–324. [PubMed: 22017877]

Duvel K, Yecies JL, Menon S, Raman P, Lipovsky AI, Souza AL, Triantafellow E, Ma Q, Gorski R, Cleaver S, et al. Activation of a metabolic gene regulatory network downstream of mTOR complex 1. Mol. Cell. 2010; 39:171–183. [PubMed: 20670887]

Fabian MR, Sonenberg N, Filipowicz W. Regulation of mRNA Translation and Stability by microRNAs. Annu. Rev. Biochem. 2010; 79:351–379. [PubMed: 20533884]

Flotow H, Graves PR, Wang AQ, Fiol CJ, Roeske RW, Roach PJ. Phosphate groups as substrate determinants for casein kinase I action. J. Biol. Chem. 1990; 265:14264–14269. [PubMed: 2117608]

Fu X-D, Ares M. Context-dependent control of alternative splicing by RNA-binding proteins. Nat. Rev. Genet. 2014; 15:689–701. [PubMed: 25112293]

Fukuhara T, Hosoya T, Shimizu S, Sumi K, Oshiro T, Yoshinaka Y, Suzuki M, Yamamoto N, Herzenberg LA, Herzenberg LA, et al. Utilization of host SR protein kinases and RNA-splicing machinery during viral replication. Proc. Natl. Acad. Sci. U. S. A. 2006; 103:11329–11333. [PubMed: 16840555]

Gammons MV, Lucas R, Dean R, Coupland SE, Oltean S, Bates DO. Targeting SRPK1 to control VEGF-mediated tumour angiogenesis in metastatic melanoma. Br. J. Cancer. 2014; 111:477–485. [PubMed: 25010863]

Gao D, Inuzuka H, Tan M-KM, Fukushima H, Locasale JW, Liu P, Wan L, Zhai B, Chin YR, Shaik S, et al. mTOR Drives Its Own Activation via SCFβTrCP-Dependent Degradation of the mTOR Inhibitor DEPTOR. Mol. Cell. 2011; 44:290–303. [PubMed: 22017875]

Ghosh G, Adams JA. Phosphorylation mechanism and structure of serine-arginine protein kinases. FEBS J. 2011; 278:587–597. [PubMed: 21205204]

Gilbert WV, Bell TA, Schaening C. Messenger RNA modifications: Form, distribution, and function. Science (80-.). 2016; 352:1408–1412.

Gomes AP, Blenis J. A nexus for cellular homeostasis: the interplay between metabolic and signal transduction pathways. Curr. Opin. Biotechnol. 2015; 34:110–117. [PubMed: 25562138]

Gonzalez Herrera KN, Lee J, Haigis MC. Intersections between mitochondrial sirtuin signaling and tumor cell metabolism. Crit. Rev. Biochem. Mol. Biol. 2015; 50:242–255. [PubMed: 25898275]

Gout S, Brambilla E, Boudria A, Drissi R, Lantuejoul S, Gazzeri S, Eymin B. Abnormal expression of the pre-mRNA splicing regulators SRSF1, SRSF2, SRPK1 and SRPK2 in non small cell lung carcinoma. PLoS One. 2012; 7:e46539. [PubMed: 23071587]

Han J, Li E, Chen L, Zhang Y, Wei F, Liu J, Deng H, Wang Y. The CREB coactivator CRTC2 controls hepatic lipid metabolism by regulating SREBP1. Nature. 2015; 524:243–246. [PubMed: 26147081]

Vander Heiden MG, Cantley LC, Thompson CB. Understanding the Warburg effect: the metabolic requirements of cell proliferation. Science. 2009; 324:1029–1033. [PubMed: 19460998]

Horton JD, Goldstein JL, Brown MS. SREBPs: activators of the complete program of cholesterol and fatty acid synthesis in the liver. J. Clin. Invest. 2002; 109:1125–1131. [PubMed: 11994399]

Howe SR, Gottardis MM, Everitt JI, Goldsworthy TL, Wolf DC, Walker C. Rodent model of reproductive tract leiomyomata. Establishment and characterization of tumor-derived cell lines. Am. J. Pathol. 1995; 146:1568–1579. [PubMed: 7539981]

Hsu PP, Kang SA, Rameseder J, Zhang Y, Ottina KA, Lim D, Peterson TR, Choi Y, Gray NS, Yaffe MB, et al. The mTOR-regulated phosphoproteome reveals a mechanism of mTORC1-mediated inhibition of growth factor signaling. Science. 2011; 332:1317–1322. [PubMed: 21659604]

Isken O, Maquat LE. The multiple lives of NMD factors: balancing roles in gene and genome regulation. Nat. Rev. Genet. 2008; 9:699–712. [PubMed: 18679436]

Jang S-W, Yang S-J, Ehlén A, Dong S, Khoury H, Chen J, Persson JL, Ye K. Serine/arginine protein-specific kinase 2 promotes leukemia cell proliferation by phosphorylating acinus and regulating cyclin A1. Cancer Res. 2008; 68:4559–4570. [PubMed: 18559500]

Jang S-W, Liu X, Fu H, Rees H, Yepes M, Levey A, Ye K. Interaction of Akt-phosphorylated SRPK2 with 14-3-3 mediates cell cycle and cell death in neurons. J. Biol. Chem. 2009; 284:24512–24525. [PubMed: 19592491]

Kamphorst JJ, Cross JR, Fan J, de Stanchina E, Mathew R, White EP, Thompson CB, Rabinowitz JD. Hypoxic and Ras-transformed cells support growth by scavenging unsaturated fatty acids from lysophospholipids. Proc. Natl. Acad. Sci. U. S. A. 2013; 110:8882–8887. [PubMed: 23671091]

Kohtz JD, Jamison SF, Will CL, Zuo P, Lührmann R, Garcia-Blanco MA, Manley JL. Protein-protein interactions and 5'-splice-site recognition in mammalian mRNA precursors. Nature. 1994; 368:119–124. [PubMed: 8139654]

Kosugi S, Hasebe M, Tomita M, Yanagawa H. Systematic identification of cell cycle-dependent yeast nucleocytoplasmic shuttling proteins by prediction of composite motifs. Proc. Natl. Acad. Sci. U. S. A. 2009; 106:10171–10176. [PubMed: 19520826]

Lee Y, Rio DC. Mechanisms and Regulation of Alternative Pre-mRNA Splicing. Annu. Rev. Biochem. 2015; 84:291–323. [PubMed: 25784052]

Li S, Brown MS, Goldstein JL. Bifurcation of insulin signaling pathway in rat liver: mTORC1 required for stimulation of lipogenesis, but not inhibition of gluconeogenesis. Proc. Natl. Acad. Sci. U. S. A. 2010; 107:3441–3446. [PubMed: 20133650]

Ma XM, Blenis J. Molecular mechanisms of mTOR-mediated translational control. Nat. Rev. Mol. Cell Biol. 2009; 10:307–318. [PubMed: 19339977]

Manning BD, Toker A. AKT/PKB Signaling: Navigating the Network. Cell. 2017; 169:381–405. [PubMed: 28431241]

Mendoza MC, Er EE, Blenis J. The Ras-ERK and PI3K–mTOR pathways: cross-talk and compensation. Trends Biochem. Sci. 2011; 36:320–328. [PubMed: 21531565]

Menendez JA, Lupu R. Fatty acid synthase and the lipogenic phenotype in cancer pathogenesis. Nat. Rev. Cancer. 2007; 7:763–777. [PubMed: 17882277]

Menon S, Manning BD. Common corruption of the mTOR signaling network in human tumors. Oncogene. 2008; 27:S43–51. [PubMed: 19956179]

Moore MJ, Proudfoot NJ. Pre-mRNA processing reaches back to transcription and ahead to translation. Cell. 2009; 136:688–700. [PubMed: 19239889]

Nardozzi JD, Lott K, Cingolani G. Phosphorylation meets nuclear import: a review. Cell Commun. Signal. 2010; 8:32. [PubMed: 21182795]

Owen JL, Zhang Y, Bae S-H, Farooqi MS, Liang G, Hammer RE, Goldstein JL, Brown MS. Insulin stimulation of SREBP-1c processing in transgenic rat hepatocytes requires p70 S6-kinase. Proc. Natl. Acad. Sci. 2012; 109:16184–16189. [PubMed: 22927400]

Park SG, Ewalt KL, Kim S. Functional expansion of aminoacyl-tRNA synthetases and their interacting factors: new perspectives on housekeepers. Trends Biochem. Sci. 2005; 30:569–574. [PubMed: 16125937]

Pascual G, Avgustinova A, Mejetta S, Martín M, Castellanos A, Attolini CS-O, Berenguer A, Prats N, Toll A, Hueto JA, et al. Targeting metastasis-initiating cells through the fatty acid receptor CD36. Nature. 2016; 541:41–45. [PubMed: 27974793]

Paz I, Kosti I, Ares M, Cline M, Mandel-Gutfreund Y, Mandel-Gutfreund Y. RBPmap: a web server for mapping binding sites of RNA-binding proteins. Nucleic Acids Res. 2014; 42:W361–7. [PubMed: 24829458]

Pearce LR, Komander D, Alessi DR. The nuts and bolts of AGC protein kinases. Nat. Rev. Mol. Cell Biol. 2010a; 11:9–22. [PubMed: 20027184]

Pearce LR, Alton GR, Richter DT, Kath JC, Lingardo L, Chapman J, Hwang C, Alessi DR. Characterization of PF-4708671, a novel and highly specific inhibitor of p70 ribosomal S6 kinase (S6K1). Biochem. J. 2010b; 431:245–255. [PubMed: 20704563]

Peterson TR, Sengupta SS, Harris TE, Carmack AE, Kang SA, Balderas E, Guertin DA, Madden KL, Carpenter AE, Finck BN, et al. MTOR complex 1 regulates lipin 1 localization to control the srebp pathway. Cell. 2011; 146:408–420. [PubMed: 21816276]

Ricoult SJH, Yecies JL, Ben-Sahra I, Manning BD. Oncogenic PI3K and K-Ras stimulate de novo lipid synthesis through mTORC1 and SREBP. Oncogene. 2016; 35:1250–1260. [PubMed: 26028026]

Rittinger K, Budman J, Xu J, Volinia S, Cantley LC, Smerdon SJ, Gamblin SJ, Yaffe MB. Structural analysis of 14-3-3 phosphopeptide complexes identifies a dual role for the nuclear export signal of 14-3-3 in ligand binding. Mol. Cell. 1999; 4:153–166. [PubMed: 10488331]

Robitaille AM, Christen S, Shimobayashi M, Cornu M, Fava LL, Moes S, Prescianotto-Baschong C, Sauer U, Jenoe P, Hall MN. Quantitative phosphoproteomics reveal mTORC1 activates de novo pyrimidine synthesis. Science. 2013; 339:1320–1323. [PubMed: 23429704]

Sanjana NE, Shalem O, Zhang F. Improved vectors and genome-wide libraries for CRISPR screening. Nat. Methods. 2014; 11:783–784. [PubMed: 25075903]

Saxton RA, Sabatini DM. mTOR Signaling in Growth, Metabolism, and Disease. Cell. 2017; 168:960–976. [PubMed: 28283069]

Schalm SS, Blenis J. Identification of a conserved motif required for mTOR signaling. Curr. Biol. 2002; 12:632–639. [PubMed: 11967149]

Selwan EM, Finicle BT, Kim SM, Edinger AL. Attacking the supply wagons to starve cancer cells to death. FEBS Lett. 2016; 590:885–907. [PubMed: 26938658]

Shimobayashi M, Hall MN. Making new contacts: the mTOR network in metabolism and signalling crosstalk. Nat. Rev. Mol. Cell Biol. 2014; 15:155–162. [PubMed: 24556838]

Siroky BJ, Yin H, Babcock JT, Lu L, Hellmann AR, Dixon BP, Quilliam LA, Bissler JJ. Human TSC-associated renal angiomyolipoma cells are hypersensitive to ER stress. Am. J. Physiol. Renal Physiol. 2012; 303:F831–44. [PubMed: 22791333]

Tani H, Akimitsu N. Genome-wide technology for determining RNA stability in mammalian cells: historical perspective and recent advantages based on modified nucleotide labeling. RNA Biol. 2012; 9:1233–1238. [PubMed: 23034600]

Thoreen CC, Kang SA, Chang JW, Liu Q, Zhang J, Gao Y, Reichling LJ, Sim T, Sabatini DM, Gray NS. An ATP-competitive mammalian target of rapamycin inhibitor reveals rapamycin-resistant functions of mTORC1. J. Biol. Chem. 2009; 284:8023–8032. [PubMed: 19150980]

Tyanova S, Temu T, Sinitcyn P, Carlson A, Hein MY, Geiger T, Mann M, Cox J. The Perseus computational platform for comprehensive analysis of (prote)omics data. Nat. Methods. 2016; 13:731–740. [PubMed: 27348712]

Wang HY, Lin W, Dyck JA, Yeakley JM, Songyang Z, Cantley LC, Fu XD. SRPK2: a differentially expressed SR protein-specific kinase involved in mediating the interaction and localization of pre-mRNA splicing factors in mammalian cells. J. Cell Biol. 1998; 140:737–750. [PubMed: 9472028]

Wang J, Wu H-F, Shen W, Xu D-Y, Ruan T-Y, Tao G-Q, Lu P-H. SRPK2 promotes the growth and migration of the colon cancer cells. Gene. 2016; 586:41–47. [PubMed: 27041240]

Yan L. Abstract #DDT01-1: MK-2206: A potent oral allosteric AKT inhibitor. Cancer Res. 2014; 69

Yu J, Astrinidis A, Howard S, Henske EP. Estradiol and tamoxifen stimulate LAM-associated angiomyolipoma cell growth and activate both genomic and nongenomic signaling pathways. Am. J. Physiol. Lung Cell. Mol. Physiol. 2004; 286:L694–700. [PubMed: 12922981]

Yu JJ, Robb VA, Morrison TA, Ariazi EA, Karbowniczek M, Astrinidis A, Wang C, Hernandez-Cuebas L, Seeholzer LF, Nicolas E, et al. Estrogen promotes the survival and pulmonary metastasis of tuberin-null cells. Proc. Natl. Acad. Sci. U. S. A. 2009; 106:2635–2640. [PubMed: 19202070]

Yu Y, Yoon S-O, Poulogiannis G, Yang Q, Ma XM, Villén J, Kubica N, Hoffman GR, Cantley LC, Gygi SP, et al. Phosphoproteomic analysis identifies Grb10 as an mTORC1 substrate that negatively regulates insulin signaling. Science. 2011; 332:1322–1326. [PubMed: 21659605]

Zhang H, Cicchetti G, Onda H, Koon HB, Asrican K, Bajraszewski N, Vazquez F, Carpenter CL, Kwiatkowski DJ. Loss of Tsc1/Tsc2 activates mTOR and disrupts PI3K–Akt signaling through downregulation of PDGFR. J. Clin. Invest. 2003; 112:1223–1233. [PubMed: 14561707]

Zhang J, Yang PL, Gray NS. Targeting cancer with small molecule kinase inhibitors. Nat. Rev. Cancer. 2009; 9:28–39. [PubMed: 19104514]

Zhang Y, Nicholatos J, Dreier JR, Ricoult SJH, Widenmaier SB, Hotamisligil GS, Kwiatkowski DJ, Manning BD. Coordinated regulation of protein synthesis and degradation by mTORC1. Nature. 2014; 513:440–443. [PubMed: 25043031]

Zheng Y, Yin H, Boeglin WE, Elias PM, Crumrine D, Beier DR, Brash AR. Lipoxygenases Mediate the Effect of Essential Fatty Acid in Skin Barrier Formation. J. Biol. Chem. 2011; 286:24046–24056. [PubMed: 21558561]

Zhou Z, Qiu J, Liu W, Zhou Y, Plocinik RM, Li H, Hu Q, Ghosh G, Adams JA, Rosenfeld MG, et al. The Akt-SRPK-SR axis constitutes a major pathway in transducing EGF signaling to regulate alternative splicing in the nucleus. Mol. Cell. 2012; 47:422–433. [PubMed: 22727668]

mTORC1-S6K1 and CK1 phosphorylate SRPK2 to induce its nuclear translocation

SRPK2 activates SR proteins and U1-70K to promote splicing of lipogenic transcripts

SRPK2 inhibition results in intron retention and lipogenic mRNA instability via NMD

Inhibition of SRPK2 signaling suppresses lipid metabolism and cancer cell growth

An mTOR-dependent pathway is a key post-transcriptional regulator of lipogenic enzymes that are involved in tumor growth.
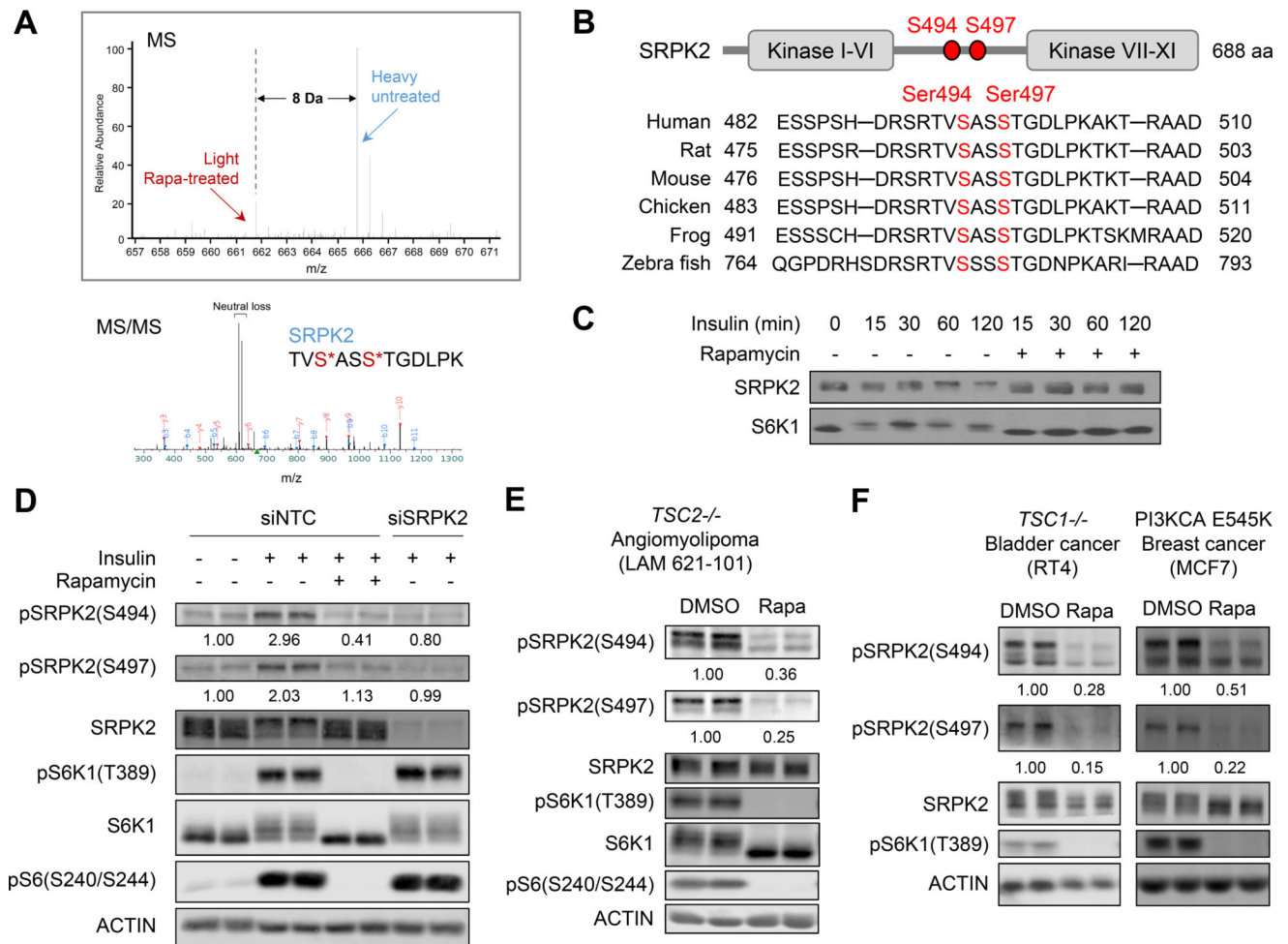
Figure 1. Identification of SRPK2 as a downstream target of mTORC1

(A) The SILAC-based phospho-proteomics analysis was performed on *Tsc2–/–* MEFs treated with vehicle or rapamycin (20 nM) for 2 hr. MS (Top) and MS/MS (Bottom) spectra of TVS*ASS*TGDLPK peptide from SRPK2 (asterisks indicate sites of phosphorylation) are shown.

(B) Schematics of SRPK2 protein domains (Top) and amino acid conservation (Bottom). The mTORC1-dependent phosphorylation sites are highlighted in red.

(C) Immunoblot analysis of HEK293E cells treated with insulin (100 nM) with or without rapamycin (Rapa, 20 nM) pre-treatment for 30 min after overnight serum starvation.

(D) Immunoblot analysis of HEK293E cells transfected with siRNAs targeting *SRPK2* or control. Cells were serum starved overnight and treated with insulin (100 nM) for 2 hr with or without rapamycin (20 nM) pre-treatment for 30 min.

(E, F) Immunoblot analysis of cancer cell lines treated with rapamycin (100 nM) for 24 hr with serum starvation. pSRPK2(S494) detects two bands in these cells.
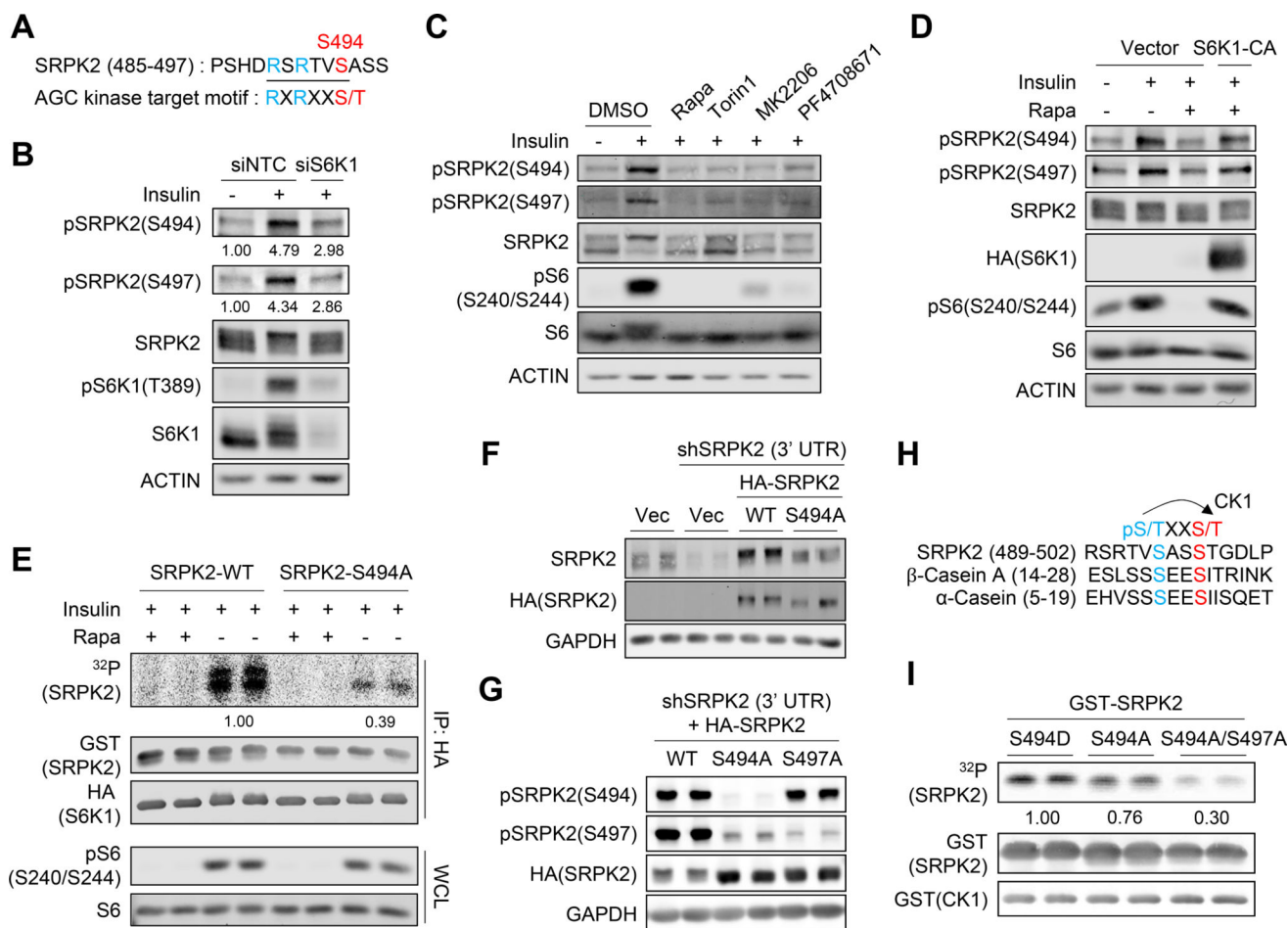
Figure 2. SRPK2 phosphorylation at Ser494 by S6K1 primes Ser497 phosphorylation by CK1
(A) Alignment of SRPK2 amino acid sequence with AGC kinase phosphorylation motif.
(B) Immunoblot analysis of HEK293E cells transfected with siRNAs targeting *S6K1* or control. Cells were treated with insulin (100 nM) for 2 hr after overnight serum starvation.
(C) Immunoblot analysis of HEK293E cells. Cells were serum starved overnight and treated with the indicated small molecule inhibitors for 30 min, followed by insulin (100 nM) treatment for 2 hr. Rapamycin (100 nM), Torin1 (250 nM), MK2206 (10 μM), and PF4708671 (10 μM) were used.
(D) Immunoblot analysis of HEK293E cells transfected with HA-S6K1-CA (constitutively active S6K1) or vector. Cells were serum starved overnight and treated with insulin (100 nM) for 2 hr with or without rapamycin (20 nM) pre-treatment for 30 min.
(E) HEK293E cells transfected with HA-S6K1 were serum starved overnight and treated with insulin (100 nM) for 2 hr with or without rapamycin (20 nM) pretreatment for 30 min. In vitro kinase essay was performed using HA-S6K1 immunoprecipitated (IP) from these cells. Recombinant GST-SRPK2-wild-type (WT) and S494A proteins were used as substrates. WCL, whole cell lysates.
(F, G) Immunoblot analysis of LAM 621-101 cells expressing HA-SRPK2-WT, S494A, or S497A. Endogenous *SRPK2* was knocked down with shSRPK2 targeting 3' UTR.

(H) Alignment of SRPK2 amino acid sequence with Casein sequences corresponding to the conserved CK1 substrate motif.
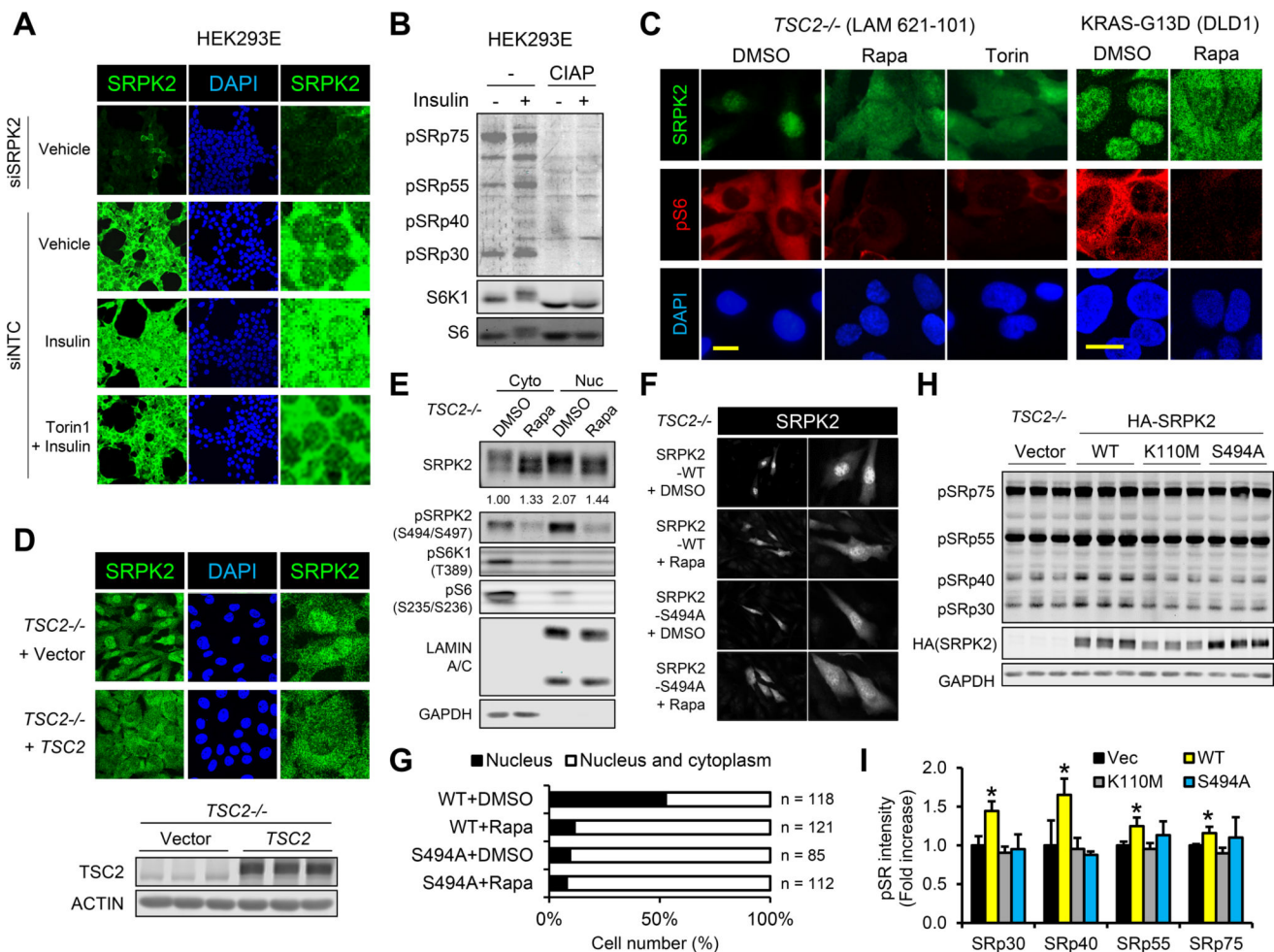
(I) In vitro CK1 kinase assay with recombinant GST-SRPK2-S494D, S494A, and S494A/S497A proteins as substrates.

Figure 3. mTORC1-dependent phosphorylation of SRPK2 induces its nuclear translocation and SR protein phosphorylation

(A) Immunostaining of SRPK2 (green) in HEK293E cells transfected with siRNAs targeting *SRPK2* or control. Cells were serum starved overnight and treated with insulin (100 nM) for 2 hr with or without Torin1 (250 nM) pre-treatment for 30 min. Right panels show the enlarged images of the white boxes in the left panels. DAPI (blue), nucleus. Scale bar, 50 μm.

(B) Immunoblot analysis of HEK293E cells treated with insulin (100 nM) for 2 hr after overnight serum starvation. Half of the cell lysates were treated with CIAP to dephosphorylate proteins.

(C) Immunostaining of SRPK2 (green) and pS6-S235/S236 (red) in the indicated cell lines treated with rapamycin (20 nM) or Torin1 (250 nM) for 2 hr. DAPI (blue), nucleus. Scale bars, 10 μm.

(D) Top, Immunostaining of SRPK2 (green) in LAM 621-101 cells (*TSC2*–/–) reconstituted with empty vector or *TSC2*. Right panels show the enlarged images of the white boxes in the left panels. DAPI (blue), nucleus. Scale bar, 50 μm. Bottom, Immunoblot analysis of the reconstituted cells.

(E) Immunoblot analysis of cytoplasmic (Cyto) and nuclear fractions (Nuc) of LAM 621-101 cells treated with rapamycin (100 nM) for 4 hr after overnight serum starvation.

(F) Immunostaining of SRPK2 (white) in LAM 621-101 cells expressing SRPK2-WT or S494A. Endogenous *SRPK2* was knocked down with shSRPK2 targeting 3' UTR. Cells were treated with vehicle or rapamycin (20 nM) for 2 hr. Right panels show the enlarged images of the white boxes in the left panels. Scale bar, 50 μm.

(G) Quantification of nuclear-cytoplasmic distribution of SRPK2 in (F). The number of cells counted is indicated.

(H) Immunoblot analysis of LAM 621-101 cells transfected with HA-SRPK2-WT, K110M (kinase dead), or S494A.

(I) Quantification of the average band intensity of phosphorylated SR proteins normalized to GAPDH in (H). n = 3. *p < 0.05.

See also Figure S1.
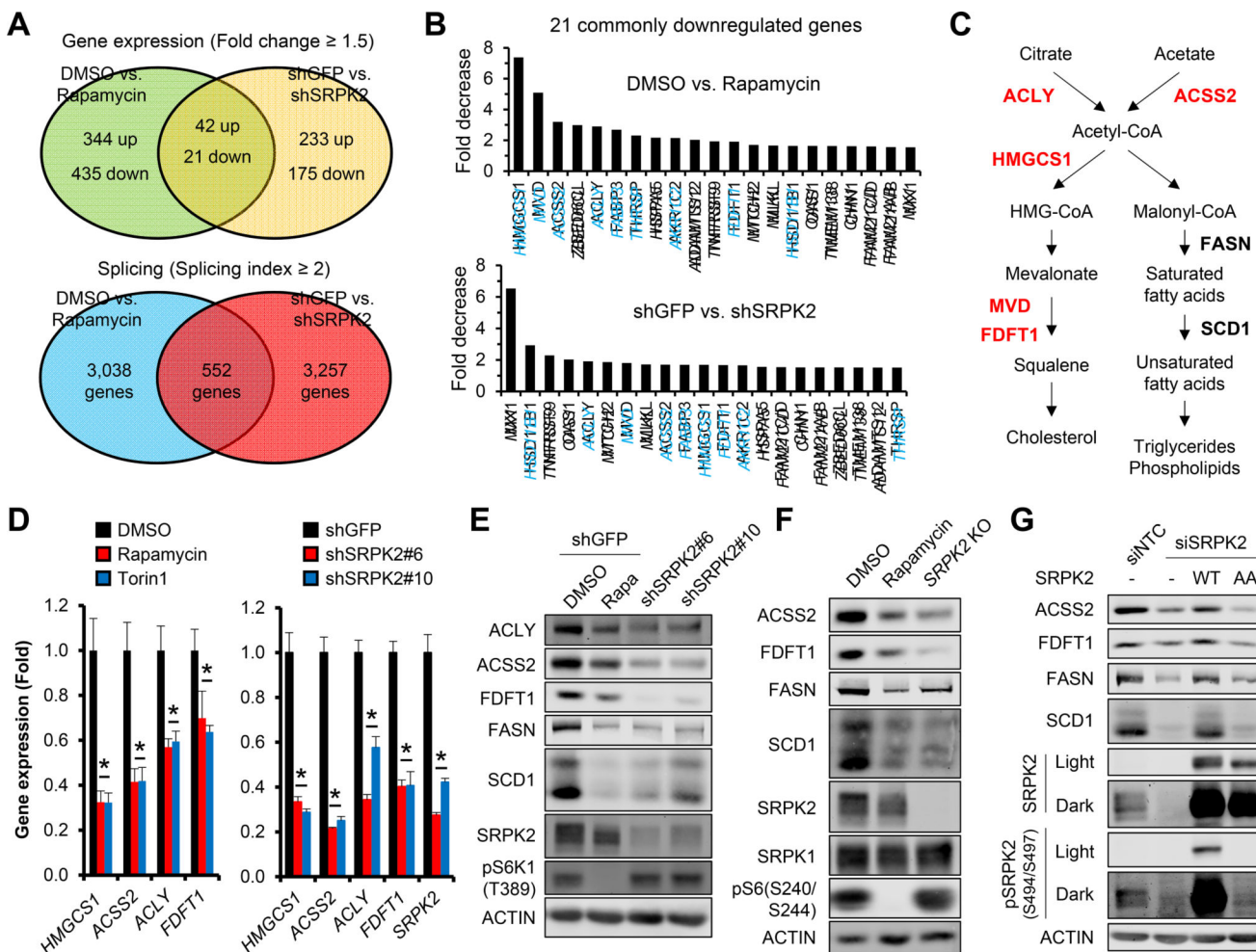
Figure 4. mTORC1 and SRPK2 signaling regulates expression of genes involved in de novo lipid synthesis

(A) Venn diagrams of the differentially regulated transcripts identified from the whole transcriptome microarray analysis on LAM 621-101 cells. One analysis was conducted on the conditions where cells were treated with rapamycin (20 nM) or vehicle for 24 hr. The second analysis was conducted on the conditions where cells stably express shRNAs targeting *SRPK2* or *GFP*. Fold cut-off for the gene expression change (linear fold change) or splicing index (SI) is 1.5 or 2, respectively. SI = [Condition 1 (Probe intensity/Gene intensity)] / [Condition 2 (Probe intensity/Gene intensity)]. n = 3. P < 0.05.

(B) Fold decreases of 21 commonly downregulated genes identified from the microarray analysis. Genes involved in lipid metabolism are highlighted in blue.

(C) Schematics of de novo lipogenesis. Genes identified from the microarray are highlighted in red.

(D) qPCR analysis of lipogenic genes in LAM 621-101 cells. Cells were treated with vehicle, rapamycin (20 nM), or Torin1 (250 nM) for 24 hr with serum starvation (left). Cells stably expressing shRNAs targeting *SRPK2* or *GFP* were serum starved overnight (right). n = 3. *p < 0.05.

(E) Immunoblot analysis of LAM 621-101 cells stably expressing shRNAs targeting *SRPK2* or *GFP*. Cells were treated with rapamycin (20 nM) or vehicle for 24 hr with serum starvation.

(F) Immunoblot analysis of LAM 621-101 cells treated with rapamycin (100 nM) or vehicle for 24 hr with serum starvation. *SRPK2* KO, *SRPK2* CRISPR knockout cells.

(G) Immunoblot analysis of LAM 621-101 cells stably expressing mouse Srpk2-WT (wild type) or AA (S488A/S491A which corresponds to S494A/S497A in human SRPK2). Cells were transfected with siRNAs targeting *SRPK2* or control and serum-starved overnight. See also Figure S2.
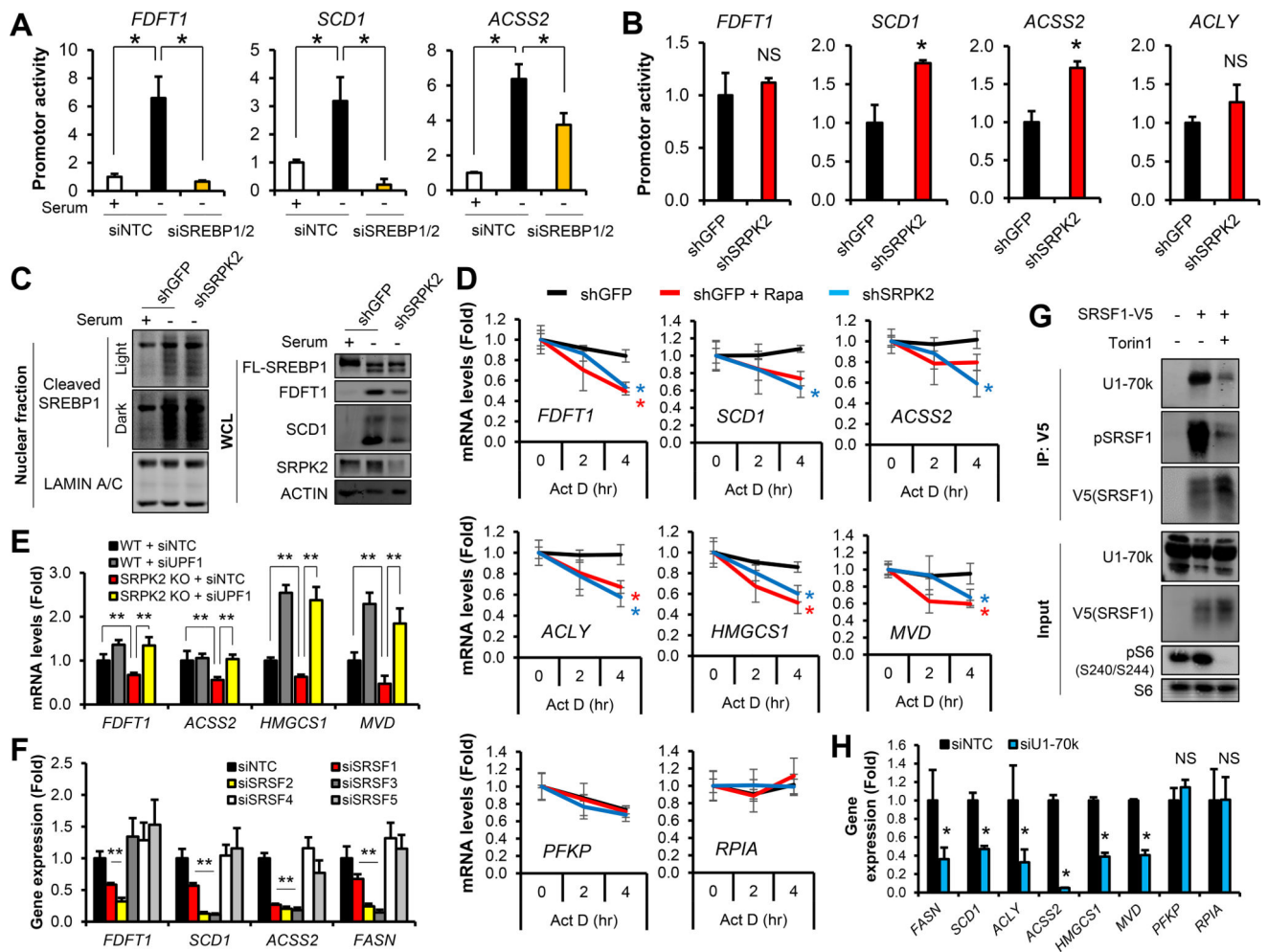
Figure 5. mTORC1 and SRPK2 signaling regulates mRNA stability of lipid biosynthetic genes

(A) Promoter activity analysis of LAM 621-101 cells transfected with promoter constructs with siRNAs targeting *SREBP1* and *SREBP2* (siSREBP1/2) or control in the presence or absence of serum. Promoter activity measured by renilla luciferase was normalized by cypridine luciferase. n = 2.

(B) Promoter activity analysis of LAM 621-101 cells stably expressing shRNAs targeting *SRPK2* or *GFP* in the absence of serum. n = 2.

(C) Immunoblot analysis of nuclear fractions or whole cell lysates (WCL) in LAM 621-101 cells in the presence or absence of serum. FL-SREBP1, full-length SREBP1.

(D) Measurement of mRNA stability in LAM 621-101 cells stably expressing shRNAs targeting *SRPK2* or *GFP*. Cells were serum starved for 24 hr with rapamycin (100 nM) or vehicle treatment, followed by actinomycin D (Act D, 5 μg/ml) treatment for the indicated time points. qPCR was performed to measure mRNA levels of the indicated genes. n = 3.
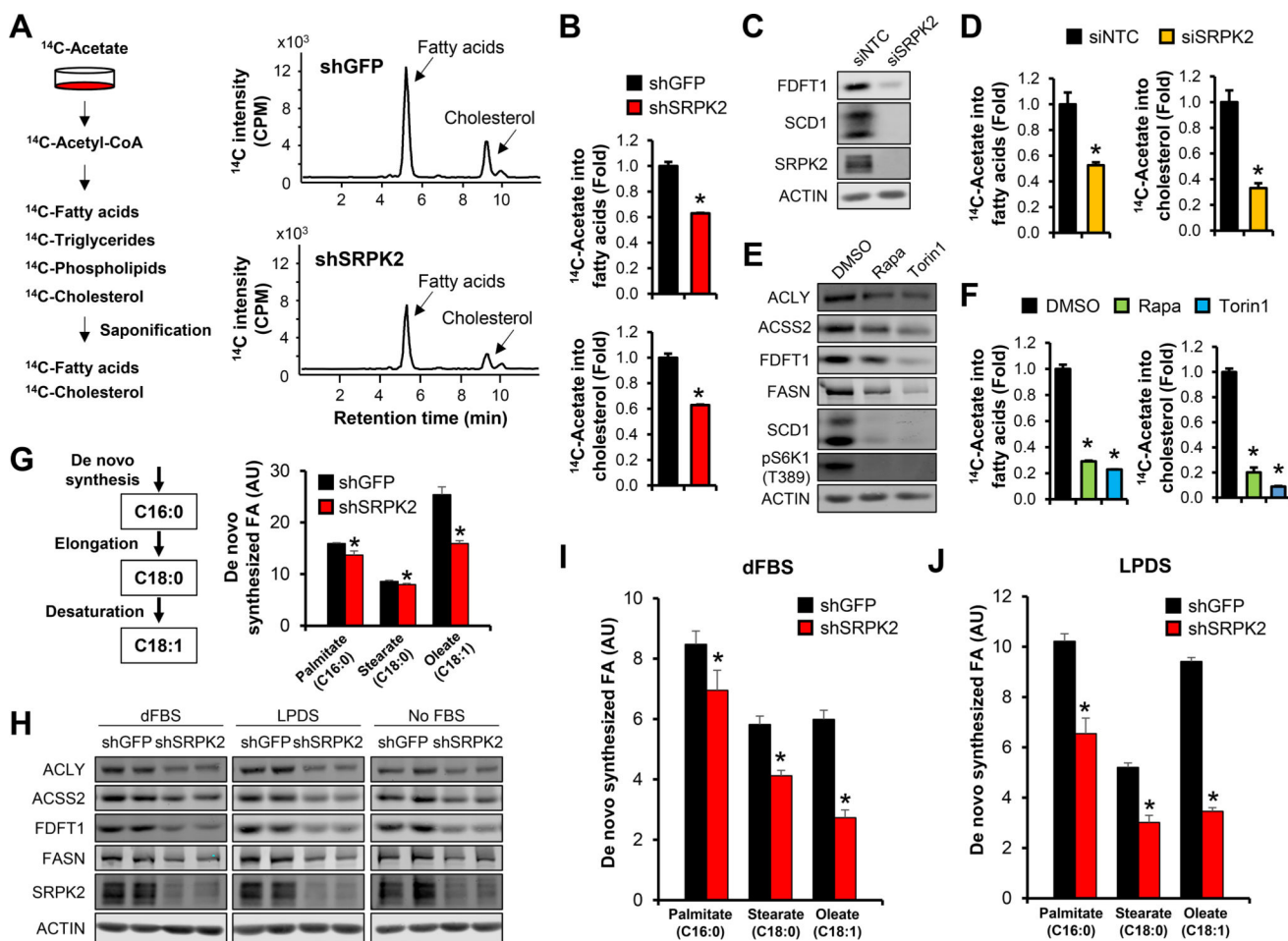
(E) qPCR analysis of WT or *SRPK2* knockout (KO) LAM 621-101 cells transfected with siRNAs targeting *UPF1* or control. n = 3.

(F) qPCR analysis of LAM 621-101 cells transfected with siRNAs targeting each *SRSF* or control. n = 3.

(G) Immunoblot analysis of HEK293E cells transfected with empty vector or SRSF1-V5. Cells were treated with Torin1 (250 nM) or vehicle for 4 hr. Immunoprecipitation (IP) was performed with anti-V5 antibody. 2% total cell lysate was loaded as an input.

(H) qPCR analysis of LAM 621-101 cells transfected with siRNAs targeting *U1-70k* or control. n = 3.

*p < 0.05 and **p < 0.01. NS, not significant. See also Figures S3 and S4 and Tables S1 and S2.

Figure 6. SRPK2 is necessary for de novo fatty acid and cholesterol synthesis

(A) Left, Schematic of radioactive ^{14}C-acetate incorporation assay for de novo fatty acid and cholesterol synthesis. Cells were cultured in serum-free medium. Right, HPLC analysis of radio-labeled fatty acids and cholesterol in LAM 621-101 cells stably expressing shRNAs targeting *SRPK2* or *GFP*.

(B) Quantification of integrated peak areas in (A) normalized to internal standard 13(S)-HODE. n = 2.

(C, E) Immunoblot analysis of LAM 621-101 cells transfected with siRNAs targeting *SRPK2* or control (C). Cells were treated with rapamycin (20 nM) or Torin1 (250 nM) for 24 hr (E).

(D, F) Radioactive ^{14}C-acetate incorporation into fatty acids and cholesterol in LAM 621-101 cells transfected with siRNAs targeting *SRPK2* or control (D). Cells were treated with rapamycin (20 nM) or Torin1 (250 nM) for 24 hr (F). Graphs represent quantification of integrated HPLC peak areas normalized to internal standard 13(S)-HODE. n = 2.

(G) LC-MS analysis of de novo fatty acid synthesis from U-^{13}C-glucose. LAM 621-101 cells stably expressing shRNAs targeting *SRPK2* or *GFP* were serum starved for 48 hr. Left, Schematics of de novo fatty acid synthesis. Right, Graph represents de novo synthesized fatty acids (FA). n = 4. Arbitrary unit (AU).

(H) Immunoblot analysis of LAM 621-101 cells stably expressing shRNAs targeting *SRPK2* or *GFP*. Cells were grown without or with 10% dialyzed FBS (dFBS) or lipoprotein-deficient serum (LPDS) for 48 hr.

(I, J) LC-MS analysis of de novo fatty acid synthesis from U-^{13}C-glucose. LAM 621-101 cells stably expressing shRNAs targeting *SRPK2* or *GFP* were grown with 10% dFBS (I) or LPDS (J). Graphs represent de novo synthesized fatty acids. n = 4.

*p < 0.05. See also Figure S5.
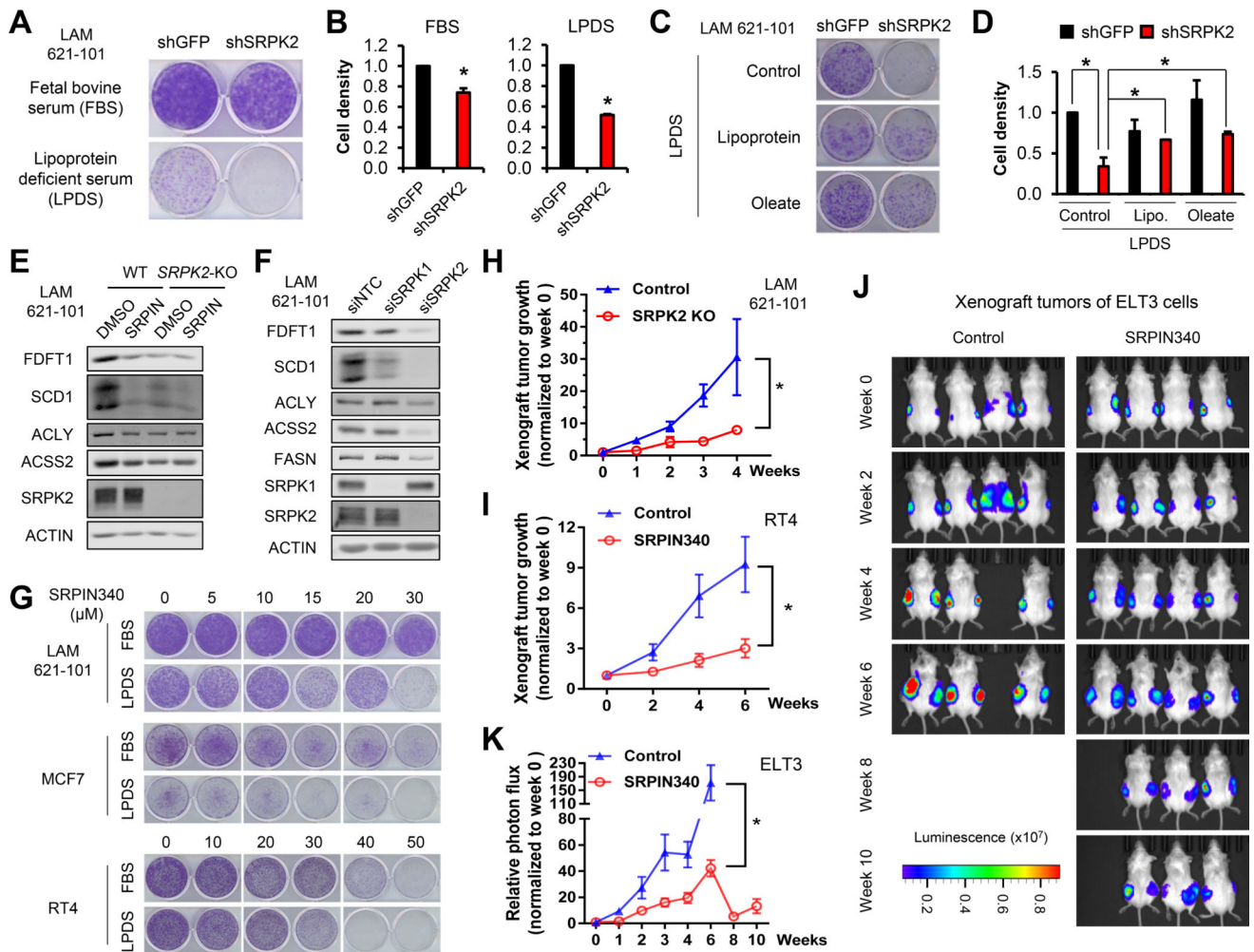
Figure 7. Inhibition of SRPK2 blunts cell growth upon lipid starvation

(A, C) Crystal violet staining of LAM 621-101 cells stably expressing shRNAs targeting *SRPK2* or *GFP*. Lipoprotein (25 μg/ml), oleate-albumin (50 μM; oleate), or fatty acid-free albumin (25 μM; control) was supplemented to the media.

(B, D) Quantification of (A) and (C), respectively.

(E) Immunoblot analysis of WT or *SRPK2* knockout (KO) LAM 621-101 cells treated with SRPIN340 (30 μM) for 48 hr with serum starvation.

(F) Immunoblot analysis of LAM 621-101 cells transfected with siRNAs targeting *SRPK1*, *SRPK2*, or control.

(G) Crystal violet staining of the indicated cell lines treated with SRPIN340 at the indicated concentrations.

(H) Xenograft tumor growth assays of WT (control) or *SRPK2* knockout (KO) LAM 621-101 cells. Graph represents the fold change of tumor size relative to week 0 (week 0 = tumor formation). n = 8 tumors.

(I–K) Xenograft tumor growth assays of RT4 (I) and ELT3 (*Tsc2–/–* rat leiomyoma)-luciferase cells (J, K) treated with SRPIN340. (I) Graph represents the fold change of tumor size relative to week 0. (J) Bioluminescent imaging of mice bearing ELT3-luciferase tumors.

(K) Graph represents the fold change of total photon flux relative to week 0 in (J). n = 6–8 tumors.

*p < 0.05. See also Figures S6 and S7.